nature cell biology

ARTICLES

Modular activation of Rho1 by GPCR signalling imparts polarized myosin II activation during morphogenesis

Stephen Kerridge[1,2,3], Akankshi Munjal[1,2], Jean-Marc Philippe[1], Ankita Jha[1], Alain Garcia de las Bayonas[1], Andrew J. Saurin[1] and Thomas Lecuit[1,3]

Polarized cell shape changes during tissue morphogenesis arise by controlling the subcellular distribution of myosin II. For instance, during *Drosophila melanogaster* gastrulation, apical constriction and cell intercalation are mediated by medial–apical myosin II pulses that power deformations, and polarized accumulation of myosin II that stabilizes these deformations. It remains unclear how tissue-specific factors control different patterns of myosin II activation and the ratchet-like myosin II dynamics. Here we report the function of a common pathway comprising the heterotrimeric G proteins $G\alpha_{12/13}$, Gβ13F and Gγ1 in activating and polarizing myosin II during *Drosophila* gastrulation. $G\alpha_{12/13}$ and the Gβ13F/γ1 complex constitute distinct signalling modules, which regulate myosin II dynamics medial–apically and/or junctionally in a tissue-dependent manner. We identify a ubiquitously expressed GPCR called Smog required for cell intercalation and apical constriction. Smog functions with other GPCRs to quantitatively control G proteins, resulting in stepwise activation of myosin II and irreversible cell shape changes. We propose that GPCR and G proteins constitute a general pathway for controlling actomyosin contractility in epithelia and that the activity of this pathway is polarized by tissue-specific regulators.

During tissue morphogenesis, cells rearrange their contacts to invaginate, intercalate, delaminate or divide[1,2]. During *Drosophila* gastrulation, invagination of the presumptive mesoderm in the ventral region of the embryo and of the posterior midgut requires apical cell constriction[3–5], a geometric deformation that occurs in different organisms[6]. Elongation of the ventral–lateral ectoderm requires cell intercalation, a general topological deformation associated with junction remodelling[7]. In the ectoderm, the so-called 'vertical junctions', oriented along the dorsal–ventral axis, shrink, followed by extension of new 'horizontal' junctions along the anterior–posterior axis[8–10]. Despite differences in the cell deformations associated with intercalation and apical constriction, recent studies revealed that both processes require myosin II (MyoII) contractility[5,8,9,11–14]. More recently, it was found that cell shape changes rely on the pulsatile activity of MyoII in the apical–medial cortex, whereby MyoII undergoes cycles of assembly and disassembly allowing stepwise deformation[15–18]. Moreover, each step of deformation is stabilized and thereby retained, contributing to the irreversibility of tissue morphogenesis[17,19–21]. In the mesoderm, each phase of apical area constriction mediated by MyoII pulses is followed by a phase of shape stabilization involving persistence of medial MyoII (ref. 20). In the ectoderm, medial–apical MyoII pulses flow anisotropically towards vertical junctions resulting in steps of shrinkage that are stabilized by a planar-polarized pool of junctional MyoII (ref. 21). This ratchet-like behaviour of MyoII is regulated by the Rho1–Rok pathway[22–27] and requires quantitative control over MyoII activation[22]. Low Rho1/Rok activity fails to form actomyosin networks, intermediate activation establishes MyoII pulsatility and high activation confers stability[22]. The signalling mechanisms that cause stepwise activation of MyoII by Rho1 remain unknown. It is also unclear whether different pathways for Rho1 activation operate in the mesoderm and in the ectoderm as indeed Rho1 can be activated by numerous signalling mechanisms[28] or whether a common pathway might exist.

Tissue-specific factors can result in polarized shape changes by signalling through cell surface receptors[29–31]. For instance, in *Drosophila* ectoderm, pair rule genes encoding transcription factors control planar-polarized enrichment of MyoII (refs 8,32) through the combinatorial expression of the surface proteins Toll2, Toll6 and Toll8 in stripes[33]. Likewise, in the mesoderm, Twist and Snail induce expression of Fog, a secreted ligand[5,19,20,34], and a G-protein-coupled receptor (GPCR) Mist, which is reported to transduce Fog (refs 35,36). The downstream G protein $G\alpha_{12/13}$ (known as Concertina (Cta) in *Drosophila*[37] and hereafter called $G\alpha_{12/13}$ (ref. 34)) is required for RhoGEF2 (ref. 38) and thereby MyoII apical recruitment[39,40]. As RhoGEF2 is a known GEF for Rho1, the requirement of $G\alpha_{12/13}$ for RhoGEF2 apical recruitment suggests that GPCRs and G-protein

[1]Aix Marseille Université, CNRS, IBDM UMR7288, 13009 Marseille, France. [2]These authors contributed equally to this work.
[3]Correspondence should be addressed to S.K. or T.L. (e-mail: stephen.kerridge@univ-amu.fr or thomas.lecuit@univ-amu.fr)

Received 30 September 2015; accepted 17 December 2015; published online 18 January 2016; DOI: 10.1038/ncb3302

signalling mediate MyoII activation through the Rho1 pathway. These considerations prompted us to ask whether G-protein signalling directly controls the different regimes of MyoII dynamics (pulsatility and/or stability) in the mesoderm and planar polarized activation of Rho1 and MyoII in the ectoderm.

Here we report the function of the heterotrimeric G proteins $G\alpha_{12/13}$, Gβ13F and Gγ1 in activating and regulating MyoII dynamics both in the mesoderm and in the ectoderm. Receptor activation, through the GEF activity of the GPCR, converts Gα from an inactive GDP-bound state, in a complex with Gβγ, to an active GTP-bound state. This results in dissociation of Gβγ, enabling binding of both Gα–GTP and Gβγ to their respective effectors for signalling (reviewed in refs 41,42). We find that $G\alpha_{12/13}$ and the Gβ13F/Gγ1 complex constitute distinct signalling modules, which regulate MyoII dynamics medial–apically and/or junctionally in a tissue-dependent manner. We identify a ubiquitously expressed GPCR called Smog, required for cell shape changes associated with both mesoderm invagination and ectoderm elongation. During these morphogenetic events, Smog functions with other GPCRs, Mist in the mesoderm and an as yet unknown GPCR in the ectoderm, to activate the Rho1–Rok pathway. This results in stepwise activation of Rho1 and MyoII, ensuring irreversible cell shape changes.

Modular activation of MyoII by Gα and Gβ/γ

We first compared the requirement for $G\alpha_{12/13}$ and Gβ13F/Gγ1 in controlling MyoII dynamics in the mesoderm and the ectoderm. We studied null mutants (see Methods) expressing E-cadherin::GFP at the locus[43] to mark cell contacts, and MyoII regulatory light chain fused to mCherry (hereafter called MyoII::Cherry[44]). In the mesoderm, *Gα12/13*, *Gβ13F* and *Gγ1* mutants resulted in failure of apical constriction and loss of medial MyoII accumulation compared with controls (Fig. 1a–h and Supplementary Fig. 1a and Supplementary Videos 1–3). In the ectoderm, the mutants of the three G proteins resulted in reduced extension (Fig. 3c,d) and junction shrinkage compared with controls (Fig. 1l–n and Supplementary Videos 4–6). Interestingly, although *Gβ13F* and *Gγ1* mutants showed loss of MyoII accumulation both medial–apically and at the junctions compared with controls (Fig. 1i,j,o,p and Supplementary Fig. 1b), $G\alpha_{12/13}$ mutants exhibited specific loss of medial–apical MyoII with no effect on MyoII accumulation at the junctions (Fig. 1k,o,p). This indicated that $G\alpha_{12/13}$ and the downstream signalling cascade are specifically required for medial activation of MyoII both in the mesoderm and in the ectoderm.

In the mesoderm, it is known that $G\alpha_{12/13}$ is required for RhoGEF2 apical localization[38] and thereby MyoII activation[39,40]. In the light of $G\alpha_{12/13}$ function in the ectoderm, we tested whether the function of apical recruitment of MyoII by RhoGEF2 is conserved in the ectoderm by making germline clones with a null allele and by doing RNAi (Methods). Both RNAi and germline clones resulted in reduced GBE, although the phenotype for the latter was stronger (Supplementary Fig. 2a). Like *Gα12/13* mutants (Fig. 1p), RNAi against *RhoGEF2* resulted in specific loss of medial–apical MyoII and no loss of junctional MyoII (Fig. 2a,b,e,f). Remarkably, overexpression of RhoGEF2 enhanced apical recruitment of MyoII (Supplementary Fig. 2b). This phenotype was very similar to the overexpression of a constitutively active form of Rho1 (RhoV14; ref. 22). We next overexpressed a constitutively active form of $G\alpha_{12/13}$, $G\alpha_{12/13}^{Q303L}$, that locks $G\alpha_{12/13}$ in a GTP-bound state[45]. Consistent with $G\alpha_{12/13}$ signalling medial–apically, $G\alpha_{12/13}^{Q303L}$ resulted in strong accumulation of MyoII medial–apically compared with controls (Fig. 2a,c,f). We next tested whether, similar to mesoderm, medial–apical activation of MyoII by RhoGEF2 is downstream of $G\alpha_{12/13}$ in the ectoderm. Strikingly, co-expression of RNAi against *RhoGEF2* with $G\alpha_{12/13}^{Q303L}$ mutants rescued the increased medial–apical accumulation of MyoII caused by the latter (Fig. 2d). Medial–apical MyoII levels were similar to *RhoGEF2* RNAi (Fig. 2f). This rescue was not observed following RNAi against *RhoGEF4*, which by itself had no defect, confirming the specificity of rescue by *RhoGEF2* RNAi (Supplementary Fig. 2c).

We conclude that the heterotrimeric G proteins $G\alpha_{12/13}$, Gβ13F and Gγ1 are required for MyoII activation both in the mesoderm and in the ectoderm suggesting the presence of GPCR signalling in the ectoderm. Although Gβ13F and Gγ1 are responsible for MyoII activation both medial–apically and at the junctions, $G\alpha_{12/13}$ and the downstream RhoGEF2 constitute a distinct signalling module responsible for medial–apical MyoII activation. This module is common in the mesoderm and in the ectoderm.

Smog is a common GPCR for mesoderm invagination and ectoderm extension

The common functions of heterotrimeric G-protein signalling in the ectoderm and mesoderm suggested that the tissue-specific activation of MyoII is under the control of tissue-specific GPCRs and/or ligands. It was recently shown that in the mesoderm, the ligand Fog signals through Mist[36], a mesoderm-specific GPCR under the control of the mesoderm-inducer Snail. We next searched for a GPCR that functions in the ectoderm to activate G-protein signalling. A region on chromosome 2 is particularly rich in genes required for gastrulation[46]. It includes the gene *CG31660*, hereafter called *smog*, which encodes for a GPCR and was incorrectly attributed to the mutant *pog* (ref. 46; Methods).

To study the function of Smog, we made a null *smog* mutant allele (hereafter called $smog^{-}$) by homologous recombination[47] (Supplementary Fig. 3a–c). In $smog^{-}$ mutants, mesoderm invagination was delayed, the posterior midgut was affected to a variable degree and, remarkably, ectoderm extension was strongly affected (Fig. 3a–d). The gastrulation mutant phenotypes were similar to *Gα12/13*, *Gβ13F* and *Gγ1* mutants (Fig. 3c), although the defects were stronger in the latter mutants. Consistent with phenotypes of $smog^{-}$ mutants in different tissues of the embryo, we found that *smog* is expressed ubiquitously in early embryos, before and during gastrulation (Fig. 3e). We conclude that Smog is a maternally expressed GPCR required for both ectoderm and mesoderm morphogenesis. This led us to test two hypotheses: Smog functions together with Mist to signal MyoII activation in the mesoderm; GPCR signalling is required for MyoII activation in the ectoderm.

The Fog–Smog/Mist pathway induces medial MyoII activation in the mesoderm

To test roles of Smog and Mist in MyoII activation in the mesoderm, we knocked down each GPCR using RNAi and made comparisons with water-injected controls (Fig. 4a–c and Supplementary Fig. 3a and Supplementary Video 7). Medial–apical MyoII::Cherry pulses in

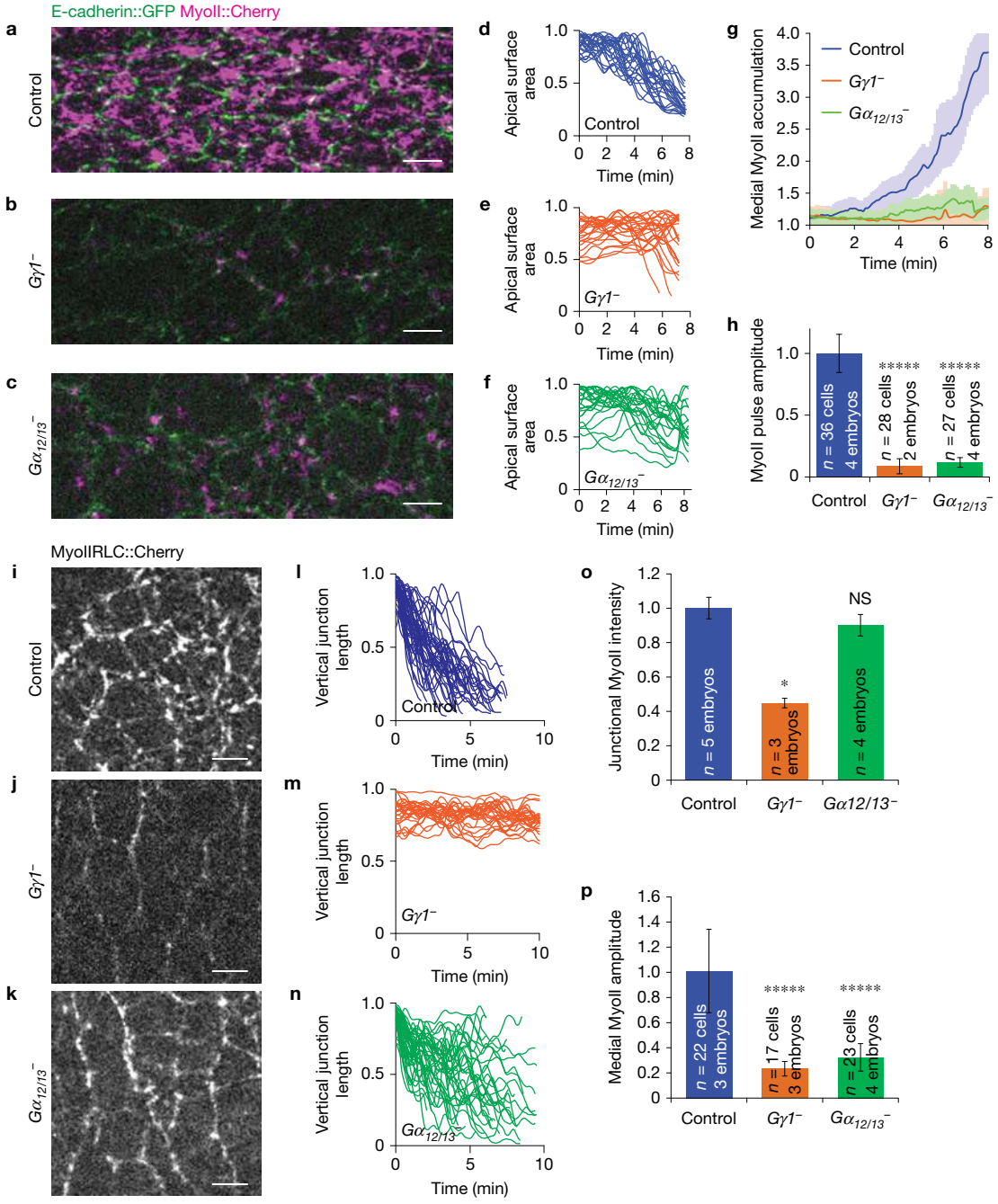

Figure 1 Heterotrimeric G proteins control MyoII dynamics in the mesoderm and ectoderm. (**a**–**c**) Apical projections of mesoderm expressing E-cad::GFP (green) and MyoII::mcherry (magenta) at 5 min post cellularization in control (**a**) and *Gγ1* (**b**) and $G\alpha_{12/13}$ (**c**) mutants. (**d**–**h**) Temporal traces of apical areas of mesoderm cells (**d**–**f**), mean medial–apical MyoII intensities (**g**) and mean pulse amplitudes (**h**) of indicated genotypes (***** $P < 0.000005$). (**i**–**k**) Apical projections of MyoII::Cherry in ectoderm cells at 25 min post cellularization. (**l**–**n**) Lengths of vertical junctions with time. (**o**) Mean junctional MyoII intensities (* $P = 0.03$ and NS, $P = 0.27$). (**p**) Mean medial pulse amplitudes in control, *Gγ1* and $G\alpha_{12/13}$ mutants in the ectoderm (***** $P < 0.000005$). All P values are calculated using the Mann–Whitney U-test. All error bars indicate s.e.m. Scale bars, 5 μm.

control embryos exhibit persistence leading to gradual accumulation of MyoII associated with apical constriction[44] (Fig. 4a,h and Supplementary Video 7). The phenotypes of RNAi against *mist* or *smog* were very similar (Fig. 4b,c and Supplementary Video 7). The medial–apical pool of MyoII was still pulsatile; however, pulses did not persist as in controls, resulting in apical area fluctuations rather than stabilized irreversible constriction (Fig. 4h,i). Consequently, invagination of the mesoderm was delayed (Fig. 4i,j). These phenotypes were different from RNAi against the ligand *fog* (Fig. 4d and Supplementary Video 8), as well as $G\alpha_{12/13}$, *Gβ13F* and *Gγ1* mutants (Fig. 1a–h and Supplementary Fig. 1a and Supplementary Videos 1–3), where besides defective MyoII persistence (Fig. 4j), MyoII pulsatility was severely affected (Fig. 4i) and invagination of the mesoderm was more strongly delayed (Fig. 4j). Consistent with

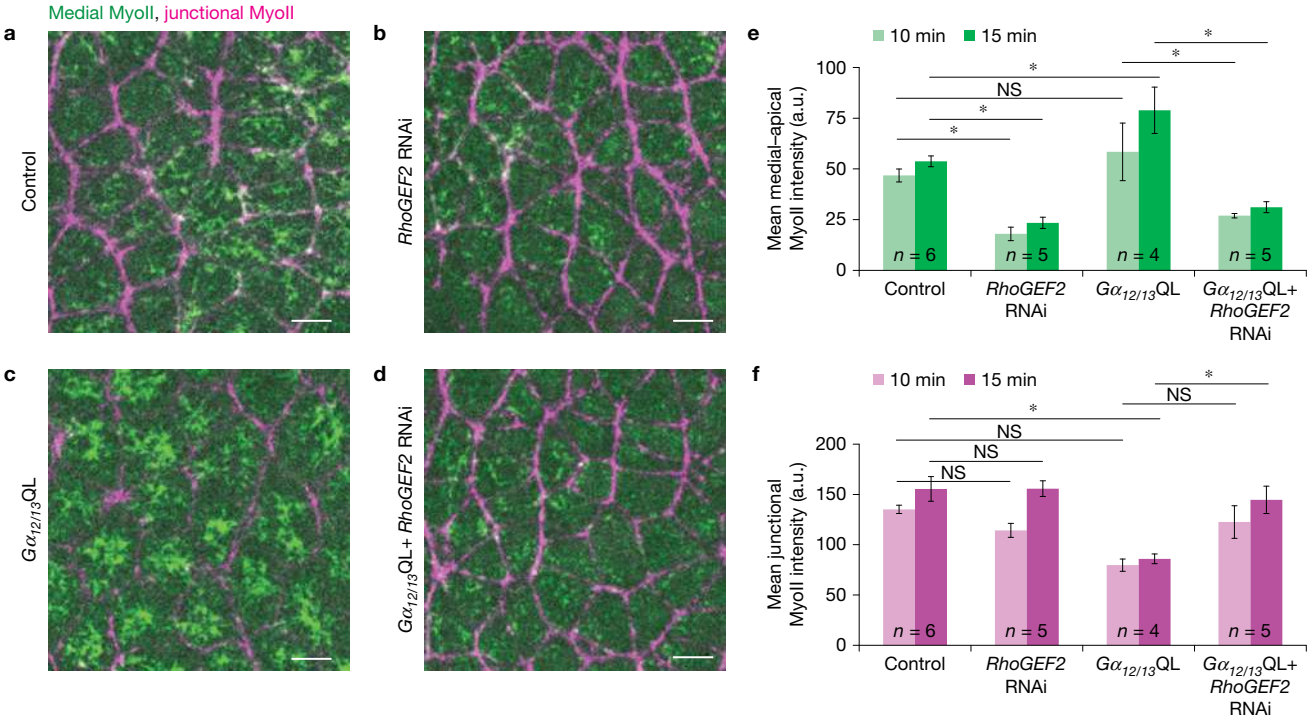

Figure 2 RhoGEF2 is required for apical–medial MyoII in the ectoderm and acts downstream of $G\alpha_{12/13}$. (**a**–**d**) Apical (green, 0–1.5 μm) and junctional (magenta, 1.5–5 μm) MyoII in control (**a**), *RhoGEF2* RNAi (**b**), activated $G\alpha_{12/13}QL303$ (**c**) and *RhoGEF2* RNAi plus $G\alpha_{12/13}QL303$ (**d**) ectoderms 25 min post cellularization. (**e**,**f**) Mean MyoII levels at the indicated times (*t*0 at 10 min post cellularization) for medial–apical regions (n = number of embryos; $^{*}P = 0.008$ between control and *RhoGEF2* RNAi for the two time points; NS, $P = 0.91$; $^{*}P = 0.04$ between control and $G\alpha_{12/13}QL303$; and $^{*}P = 0.01$ between control and $G\alpha_{12/13}QL303$ + RhoGEF2 RNAi for the two time points) (**e**) and junctional regions (n = number of embryos; NS, $P = 0.08$ and $P = 0.74$ between control and *RhoGEF2* RNAi for the two time points, respectively; NS, $P = 0.17$ between control and $G\alpha_{12/13}QL303$; $^{*}P = 0.01$ between control and $G\alpha_{12/13}QL303$; NS is $P = 0.52$ between control and $G\alpha_{12/13}QL303$ + *RhoGEF2* RNAi; and $^{*}P = 0.01$ between control and $G\alpha_{12/13}QL303$ + *RhoGEF2* RNAi for the two time points) (**f**). All P values are calculated using the Mann–Whitney U-test. All error bars indicate s.e.m. Scale bars, 5 μm.

the idea that Fog signals upstream of Mist and Smog, we found that similar to *fog* RNAi alone, RNAi against either *mist* and *fog* (Fig. 4e), or against *smog* and *fog* (Fig. 4f and Supplementary Video 8) resulted in negligible MyoII accumulation and pulsatility abrogating ventral furrow formation (Fig. 4h–j).

We further tested the hypothesis that Fog signals through Smog by expressing a fusion between Smog and GFP (Smog::GFP) in $smog^{-}$ mutant embryos (see Methods). Smog::GFP rescued the mutant phenotype similar to untagged Smog (Supplementary Fig. 4a). Smog::GFP was localized throughout the cell surface (Supplementary Fig. 4b) and also present in subcellular vesicles (Supplementary Fig. 4c). These vesicles were endocytic as Smog::GFP co-localized with internalized fluorescent dextran in the ectoderm (Supplementary Fig. 4d). In *fog* null mutants, these vesicles were less abundant in the mesoderm (Supplementary Fig. 4c). We then expressed a functional Smog::GFP fusion in *Drosophila* S2 cells in the presence of medium containing HA-tagged Fog. As in the embryo, Smog::GFP was localized at the cell surface and in intracellular vesicles in S2 cells (Supplementary Fig. 4e). Immunostaining of Fog showed that it was specifically immobilized at the surface of Smog::GFP-expressing cells and in internal vesicles but not in S2 control cells (Supplementary Fig. 4e,f). We conclude that Fog binds the cell surface in a Smog-dependent fashion and signals by inducing Smog endocytosis.

We next tested whether Fog signalling through Smog and Mist, together, is sufficient for MyoII activation in the mesoderm, by performing *smog* and *mist* double RNAi and making comparisons with *fog* RNAi (Fig. 4g and Supplementary Video 7). *smog* and *mist* double RNAi was more severe than the respective single RNAi in that MyoII accumulation was delayed, MyoII pulse amplitude was reduced and invagination of the mesoderm was abrogated (Fig. 4i,j). We conclude that Smog and Mist function additively downstream of Fog to activate G-protein signalling. Higher medial–apical MyoII levels in *mist* and *smog* double RNAi compared with *fog* RNAi (Fig. 4i) may be due to incomplete inactivation of these receptors by RNAi. However, we cannot rule out the existence of another GPCR working together with Smog and Mist to transduce Fog signalling. These data also lead us to conclude that Fog imparts apical restriction to MyoII activation through Mist and Smog in the mesoderm.

Smog is required for junctional MyoII activation in the ectoderm

We next addressed the role of Smog in MyoII activation in the ectoderm. In $smog^{-}$ mutants, like in the mesoderm, medial MyoII remained pulsatile, with even slightly higher amplitude of pulses (Fig. 5a–d and Supplementary Video 9). However, contrary to wild-type embryos, MyoII did not accumulate at cell junctions leading to defective junction shrinkage (Fig. 5e–i and Supplementary Video 9). Whereas in controls junctions shrink in a stepwise manner (Fig. 5h),

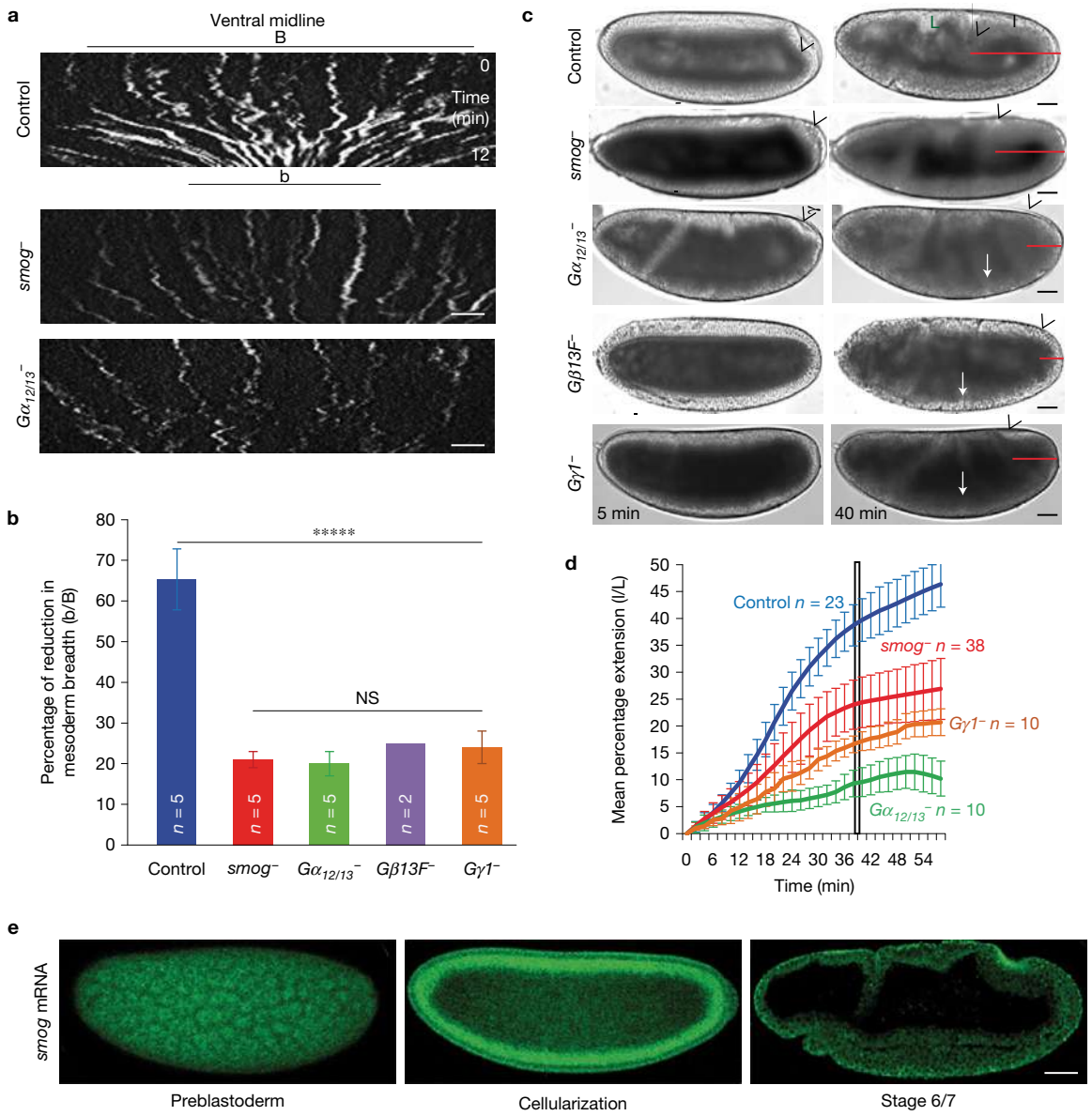

Figure 3 The ubiquitously expressed GPCR Smog and G proteins are required for both mesoderm constriction and ectoderm elongation. (**a**) 12 min kymographs of E-cad::GFP at the apical cell surface in control and *smog* and $G\alpha_{12/13}$ mutant ventral furrow cells. Note the reduction of the breadth of the mesoderm (labelled B at $t = 0$ and b at $t = 12$ min). (**b**) Quantifications of the percentage of mesoderm breadth reduction (b/B) in different genotypes (n = the number of embryos; $^{*****}P < 0.000005$ and NS, $P = 0.7$ calculated using the Mann–Whitney U-test). (**c**) Side views of wild-type and *smog*$^-$, $G\alpha_{12/13}$, and $G\beta 13F$ and $G\gamma 1$ mutants showing germband elongation. In *smog* and G-protein mutants, the anterior movement of the pole cells (arrowheads) due to posterior midgut invagination and tissue extension is defective (red lines). Arrows highlight folds in the ectoderm. (**d**) Quantification of germband extension in control and mutants (n = number of embryos). (**e**) Distribution of *smog* RNA in wild-type embryos. Scale bars, 10 μm (**c**,**e**) and 5 μm (**a**). Error bars, s.e.m. for **c** and s.d. for **d**.

in *smog*$^-$ mutants junctions fluctuated in length but did not shrink persistently (Fig. 5i). These experiments show that Smog signalling is responsible for MyoII activation at the junctions in the ectoderm. The signalling module involves Gβ13F/Gγ1, which activates MyoII at junctions (and medial–apically; Fig. 1o). The signalling module is different from the one constituted by $G\alpha_{12/13}$ and RhoGEF2 that is responsible specifically for medial–apical activation of MyoII (Figs 1o,p and 2).

This finding poses the question of how Smog results in medial–apical activation of MyoII in the mesoderm and junctional activation in the ectoderm. We suggest the existence of tissue-specific ligands to result in these differential functions. Whereas Fog is strongly expressed in the mesoderm, it is also detected, albeit at very low levels, in the ectoderm cells before intercalation[48] but its function is unclear. Fog overexpression in the ectoderm induces elevated MyoII recruitment in the medial–apical region[5] and apical cell flattening in the ectoderm cells[48]. This Fog-induced modification of MyoII accumulation is partially dependent on Smog and completely dependent on $G\alpha_{12/13}$ (Fig. 5j–n and ref. 48). Consistent with this, Smog::GFP vesicles were more numerous when Fog was overexpressed (Supplementary Fig. 4d,g) and less abundant in *fog*

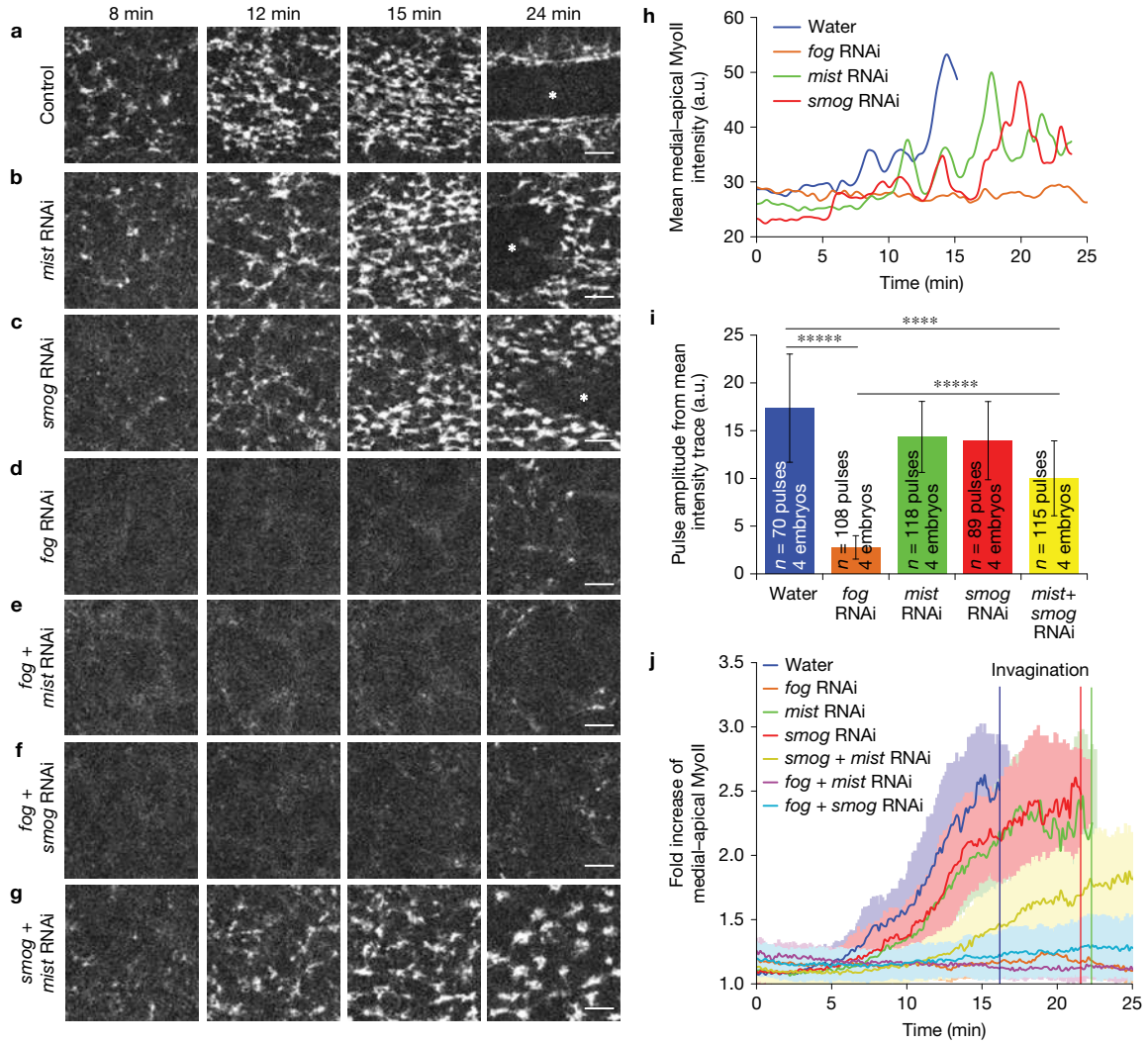

Figure 4 The Fog ligand requires at least two GPCRs, Smog and Mist, for apical MyoII accumulation in the mesoderm. (**a**–**g**) MyoII::Cherry profiles in the mesoderm of the indicated injected embryos at different times post *t*0 (see Methods); asterisks mark invaginated regions; scale bars, 5 μm. (**h**) Representative medial–apical MyoII traces. (**i**) Average pulse amplitudes ($^{*****}P = 1.14083 \times 10^{-9}$ between control and *fog* RNAi; $^{****}P = 6.51648 \times 10^{-7}$ between control and *smog*+*mist* RNAi; and $^{*****}P = 4.26837 \times 10^{-8}$ between *fog* RNAi and *smog*+*mist* RNAi). Error bars are s.e.m. (**j**) Average fold increase traces of MyoII with time of the indicated RNAi and water-injected controls. Vertical lines indicate approximate times of invagination. Error bars are s.d. All *P* values are calculated using the Mann–Whitney *U*-test. Scale bars, 5 μm.

mutants (Supplementary Fig. 4c). Moreover, *fog* mutants exhibited loss of medial–apical MyoII recruitment in the ectoderm and no loss of junctional MyoII (Fig. 5o,p,s,t), similar to $G\alpha_{12/13}$ and RhoGEF2 loss of function (Figs 1o,p and 2e,f). Interestingly, *fog* and *smog* double RNAi showed an additive phenotype in the ectoderm, whereby both medial and junctional MyoII accumulation was lost (Fig. 5r–t). These experiments indicate that the low levels of Fog in the ectoderm signal through Smog and an unknown GPCR to activate the $G\alpha_{12/13}$/RhoGEF2 module for medial–apical recruitment of MyoII.

Smog activates the Rho1 pathway

We next tested whether Smog medial–apical activation of MyoII in the mesoderm and junctional activation in the ectoderm depends on the Rho1/Rok pathway. In the mesoderm, like MyoII, Rok::GFP accumulates medial–apically and not at junctions[27] (Supplementary Fig. 5a). Strikingly, in *smog*$^{-}$ mutants, Rok::GFP levels were reduced medial–apically (Supplementary Fig. 5a). To study the localization of activated Rho1, we used the Rho1GTP sensor (Rho1sensor::GFP; ref. 22). Rho1sensor::GFP localized medial–apically like MyoII::Cherry (Supplementary Fig. 5b). In *smog* RNAi, Rho1sensor::GFP levels were reduced medial–apically (Supplementary Fig. 5b).

In contrast, in the ectoderm, MyoII is predominantly junctional and planar polarized. Enrichment of MyoII on vertical junctions requires Rho1 (ref. 25) and Rok (refs 8,23) and these proteins are themselves planar polarized (Fig. 6a,b,d–f). In *smog* RNAi, we found that the levels of Rho1sensor::GFP and Rok::GFP, like MyoII, were strongly reduced at junctions (Fig. 6a–e). Moreover, expression of a phospho-mimetic mutant of MyoIIRLC fused with GFP (MyoIIEE::GFP) rescued MyoII localization at cell junctions in *smog* RNAi embryos (Fig. 6g,h), however with perturbed planar polarity[22] (Fig. 6i). We conclude that Smog activates junctional MyoII by controlling Rho1- and Rok-dependent phosphorylation of MyoII.

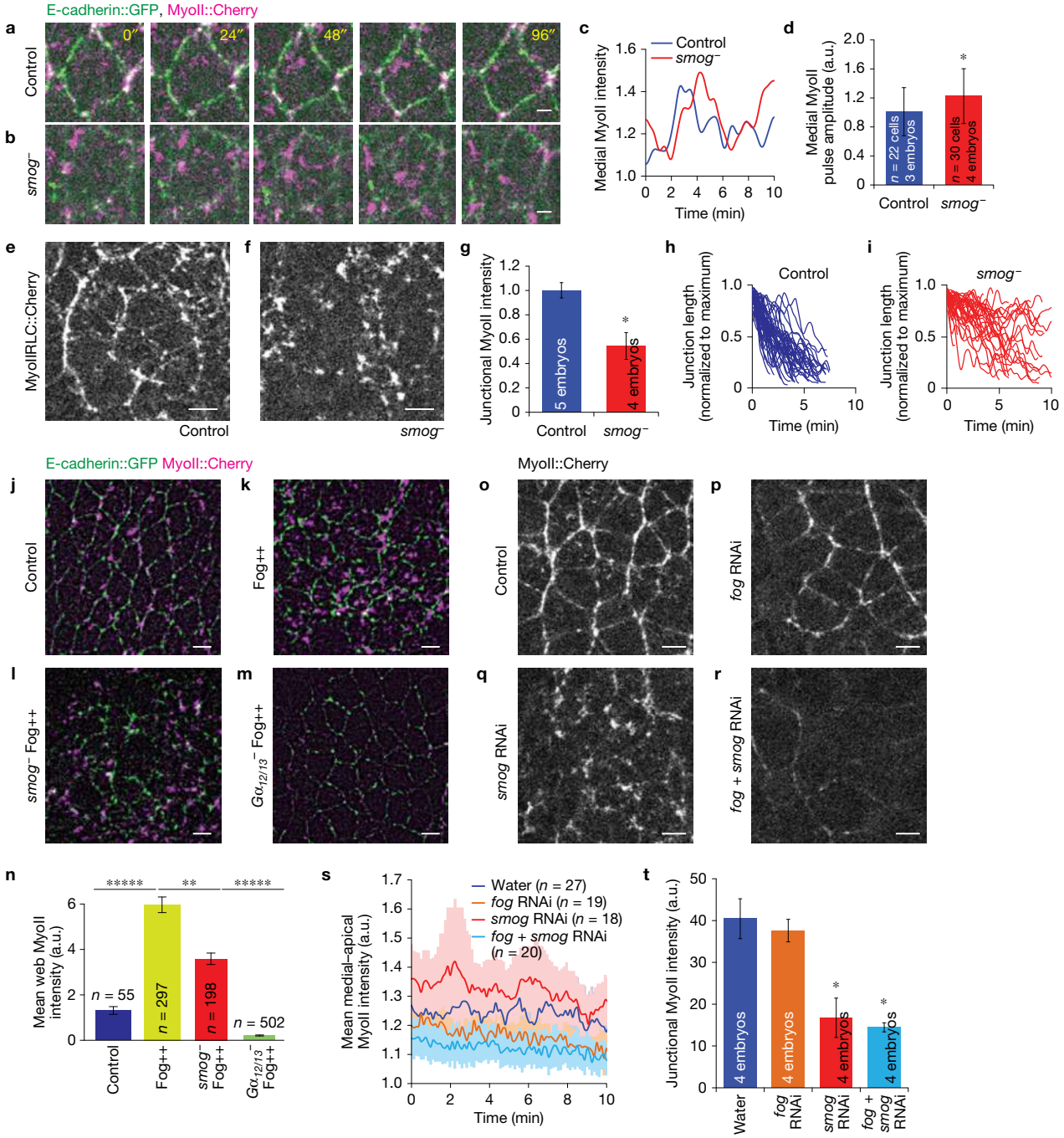

Figure 5 Smog is required in the ectoderm for MyoII distribution and contributes to Fog signalling. (**a**,**b**) Distribution of E-Cad::GFP (green) and MyoII::Cherry (magenta) in single ectoderm cells from control (**a**) and *smog*⁻ (**b**) embryos at the indicated times. (**c**,**d**) Single-cell traces of medial MyoII (**c**) and average medial MyoII pulse amplitudes (**d**) in *smog*⁻ and control amplitudes ($^{*}P = 0.04$). (**e**,**f**) Snapshots of MyoII in the indicated ectoderms at 25 min post cellularization. (**g**) Junctional MyoII levels ($^{*}P = 0.007$) (**g**) and junctional length traces (**h**,**i**) in control and *smog*⁻ mutants. (**j**–**m**) Ectoderm cells expressing MyoII::Cherry (magenta) and E-Cad::GFP (green) in control (**j**) and embryos expressing increased Fog levels (**k**–**m**) in a *smog*⁻ (**l**) or $G\alpha_{12/13}$ mutant background (**m**). (**n**) Quantification of mean medial MyoII levels in the same genotypes (n = number of cells; $^{*****}P < 0.000005$; $^{**}P = 0.005$. (**o**–**r**) MyoII::Cherry profiles in ectoderm 25 min post cellularization in control (**o**), *fog* RNAi (**p**), *smog* RNAi (**q**) and *fog* plus *smog* RNAi (**r**) embryos. (**s**,**t**) Mean medial–apical (**s**) and junctional (**t**) intensities at 25 min post cellularization. In **s**, n = number of cells. In **t**, n = number of embryos. $^{*}P = 0.01$. All P values are calculated using the Mann–Whitney U-test. Error bars are s.e.m. in **d**,**g**,**n** and **t** and s.d. in **s**. Scale bars, 1 μm (**a**,**b**) and 5 μm (**e**,**f**,**j**–**m**,**o**–**r**).

Multiple GPCRs allow stepwise activation of MyoII by Rok

It is striking that single-receptor inactivation (Smog or Mist) affects stability of MyoII but not pulsatility (Figs 4i,j and 5d,g). Interestingly, two-tiered activation of MyoII is required for establishing pulsatility (intermediate activation) and stability (strong activation[22]). This suggests that multiple GPCRs allow stepwise activation of MyoII.

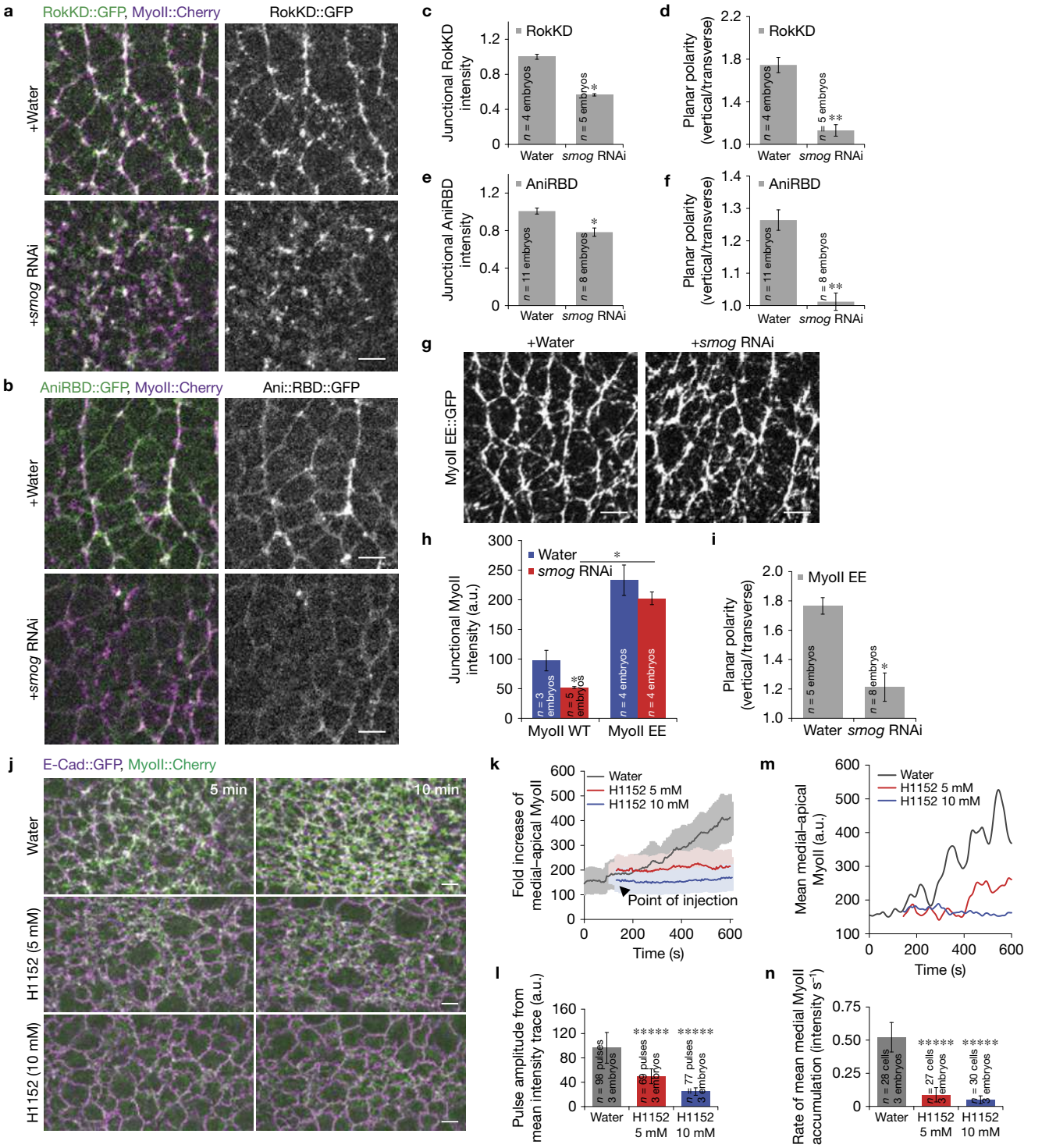

Figure 6 Smog controls Rok and Rho1 distribution in the ectoderm and mild inhibition of Rok mimics the effects of *smog* or *mist* knockdown in the mesoderm. (**a**) RokKD::GFP (KD: kinase dead; green) and MyoII::Cherry (magenta) in embryos injected with water (upper) or *smog* RNAi (lower panels). MyoII channels right. (**b**) Distribution of the Rho1GTP sensor or Anilin Rho-binding domain fused to GFP (AniRBD::GFP) (green) and MyoII::Cherry (magenta) in control (top) and *smog* RNAi (bottom) embryos. (**c**–**f**) Quantification of RokKD::GFP and AniRBD::GFP junctional levels (**c**,**e**) and planar polarity (**d**,**f**). In **c**, $^{*}P=0.01$. In **d**,**f**, $^{**}P=0.001$. In **e**, $^{*}P=0.03$. (**g**) Distribution of constitutively active MyoII fused to GFP (MyoIIEE::GFP) in the ectoderm following water (left) and *smog* RNAi (right) injection. (**h**,**i**) Quantification of junctional MyoIIWT::GFP and MyoIIEE::GFP levels (**h**) and planar polarity (**i**) in the indicated injected embryos. In **h**, $^{*}P=0.03$. In **i**, $^{*}P=0.01$. (**j**) Mesoderm showing control- (top), mild- (middle) and high-H1152- (bottom) injected embryos at two time points. (**k**–**n**) Quantifications showing fold increase (**k**), pulse amplitude (**l**), mean apical–medial (**m**) and rates (**n**) of medial–apical accumulation of MyoII in control and Rok-inhibited mesoderm cells. n = number of cells in the indicated number of embryos. $^{*****}P<0.000005$. All P values are calculated using the Mann–Whitney U-test. All error bars are s.e.m. Scale bars, 5 μm.

Knowing that Smog activates MyoII through the Rho1/Rok pathway, we tested this hypothesis in the mesoderm with an intermediate (5 mM) and strong (10 mM) inhibition of Rok by injecting a pharmacological inhibitor (H1152) at the onset of apical constriction (Stage 5a; Fig. 6j and Supplementary Video 10). We found that intermediate inhibition of Rok phenocopied *smog* or *mist* single RNAi (Fig. 4c,d and Supplementary Video 7), namely that MyoII exhibits pulsatile dynamics but does not persist to result in apical constriction (Fig. 6k–n and Supplementary Video 10). Moreover, strong inhibition of Rok (Fig. 6k–n and Supplementary Video 10) phenocopied *fog* RNAi (Fig. 4d and Supplementary Video 8) or G-protein mutants in that little or no MyoII accumulated (Fig. 1 and Supplementary Figs 1–3) abrogating apical constriction and mesoderm invagination. We conclude that multiple GPCRs allow stepwise activation of MyoII establishing pulsatility and stability to drive irreversible shape changes.

DISCUSSION

We have shown that GPCR signalling relays information conveyed by tissue-specific transcription factors in the mesoderm and ectoderm to drive shape changes during tissue morphogenesis. We report that Rho1-dependent activation of MyoII during both apical constriction and cell intercalation is controlled by a core GPCR (Smog) and heterotrimeric G-protein signalling pathway. By providing a molecular framework for the regulation of cellular mechanics in two different, generic morphogenetic processes, potentially general principles for the spatial regulation of actomyosin networks by Rho1 exist: modular activation important for polarity; and quantitative activation to specify a pulsatile or stable regime.

First, we report that $G\alpha_{12/13}$ and Gβ13F/Gγ1 function as distinct signalling modules that control Rho1 and MyoII in different domains (Supplementary Fig. 6). $G\alpha_{12/13}$ activates medial–apical MyoII through its effector RhoGEF2 both in the ectoderm and the mesoderm. In mammals, p115–RhoGEF interacts directly with $G\alpha_{12}$ (ref. 49) suggesting that this may be a conserved signalling module. In contrast, Gβ13F/Gγ1 activates MyoII both at cell junctions and in the medial–apical domain. This modularity may provide distinct regulatory mechanisms for the activation of MyoII in different subcellular compartments owing to the existence of different molecular effectors of Gα–GTP and Gβγ (ref. 41). Second, stepwise activation of Rho1 by multiple GPCRs and their ligands determines the emergence of a pulsatile regime medial–apically, or stable activation[22] (Supplementary Fig. 6). In the mesoderm, Smog and Mist GPCRs, together with high expression of their ligand Fog, ensure stabilization and rapid (<5 min) accumulation of MyoII ensuring apical constriction. In the ectoderm, low Fog expression and thus lower activation of $G\alpha_{12/13}$ and RhoGEF2 is responsible for intermediate medial–apical activation of MyoII and pulsatility. Indeed, Fog, constitutively active $G\alpha_{12/13}$QL and RhoGEF2 overexpression all lead to stable accumulation of MyoII instead of pulsation, similar to constitutively active RhoV14 (ref. 22).

Interestingly, the same receptor Smog controls MyoII activation in different subcellular domains during intercalation and apical constriction begging the question of how activation of $G\alpha_{12/13}$ and Gβγ is differentially achieved in the ectoderm and the mesoderm. The polarization of Smog activation is to some extent imparted by the ligand. Fog/Smog regulates medial–apical accumulation of MyoII in the two tissues: Fog induces medial Rho1 and Rok activation in the mesoderm and ectoderm and, when ectopically expressed in the ectoderm, it can increase Rho1 and Rok in the medial cortex. This argues that another mechanism results in junction-specific activation of Smog, Gβ13F/Gγ1, Rho1 and Rok in the ectoderm.

It is possible that an unknown ectoderm-specific ligand activates Smog specifically at junctions. Junctional localization of the Rho1 pathway by Smog may also be imparted by subcellular processing of Smog signalling, such as localization/activation of downstream effectors of $G\alpha_{12/13}$ and Gβγ. The recently identified Toll receptors[33] required for MyoII planar-polarized activation may bias Smog signalling although the molecular mechanisms remain unclear. This could be through localization of RhoGEFs. In the mesoderm, the transmembrane protein T48 localizes RhoGEF2 apically through binding to its PDZ domain, and is required for apical MyoII activation in parallel with Smog, $G\alpha_{12/13}$ and Gβγ. Similarly, other GEFs may be required for junctional Rho1 activation by Smog.

We wish to know what might be the advantage of having multiple GPCRs. Gastrulation sets the foundation for all other future processes in development and hence requires robustness. GPCRs with similar functions yet subtle differences such as ligand specificity may offer advantages compared with single ligand–receptor pairs. For instance, high cortical tension associated with mesoderm invagination may require multiple GPCRs activating parallel pathways to attain efficiency of the process. Moreover, multiple GPCRs may concede tissue-specific regulation of the common G-protein subcellular pathways. Finally, multiple GPCRs can allow stepwise activation of MyoII. Although activation by one GPCR is sufficient to induce pulsatility, more GPCRs are required to shift the actomyosin networks to more stable regimes.

The discovery that Smog and heterotrimeric G protein activate Rho1 and MyoII in two different morphogenetic processes provides a potentially general molecular framework for tissue mechanics. We propose that different developmental inputs tune a common GPCR/G-protein signalling pathway to direct specific patterns and levels of Rho1 activation. Quantitative control specifies the regime of MyoII activation through Rho1, namely pulsatility or stability of MyoII. Modular control defines the subcellular domains where MyoII accumulates (medial–apical or junctions) depending on molecular effectors (Supplementary Fig. 6). How developmental signals tune GPCR signalling will be important to decipher. □

METHODS

Methods and any associated references are available in the online version of the paper.

Note: Supplementary Information is available in the online version of the paper

ACKNOWLEDGEMENTS

We are grateful to K. Zinn (Caltech, USA), N. Fuse (Kyoto, Japan), J. Knoblich (IMBA, Austria), M. Leptin (Cologne, Germany), A. Martin (MIT, USA), V. Mirouse (Clermont, USA), E. Wieschaus (Princeton, USA), J. Zallen (Sloan-Kettering, USA), the Drosophila Genetic Resource Center and the Bloomington Stock Center for the gift of flies. A. Ratnaparkhi (IISER, India) provided plasmids. We thank D. Coiffier for the *in situ* hybridization shown in Supplementary Fig. 3e. This work benefited greatly from the stimulating discussions in the Lecuit and Lenne laboratories and from the Labex INFORM ((ANR-11-LABX-0054) under the A*MIDEX program (ANR-11-IDEX-0001-02)). This work was financially supported by the ERC (Biomecamorph no. 323027), the ANR Archiplast (Programme Blanc)

and the CNRS (S.K. and T.L.). A.M. was supported by the Ministère de l'Education nationale and the Association pour la Recherche contre le Cancer (ARC). This work was performed using the France-BioImaging infrastructure supported by the Agence Nationale de la Recherche (ANR-10-INSB-04-01, call 'Investissements d'Avenir').

AUTHOR CONTRIBUTIONS

S.K. and T.L. planned the project. S.K., A.M. and T.L. analysed the data. S.K. discovered *smog* and performed the experiments shown in Figs 1, 3–5 and Supplementary Figs 1, and 3 and 4. A.M. carried out the experiments in Figs 4–6 and the quantifications of Figs 1 and 4–6. A.G.d.l.B. performed the experiments in Fig. 2 and Supplementary Fig. 2. A.J. carried out the experiments and quantifications in Supplementary Figs 4 and 5. J.-M.P. made the constructs, cloning and molecular characterization of *smog*. A.J.S. provided unpublished materials and technical expertise for the S2 cell experiments (Supplementary Fig. 4). S.K., A.M. and T.L. wrote the paper. All authors commented on the manuscript.

COMPETING FINANCIAL INTERESTS

The authors declare no competing financial interests.

Published online at http://dx.doi.org/10.1038/ncb3302
Reprints and permissions information is available online at www.nature.com/reprints

1. Guillot, C. & Lecuit, T. Mechanics of epithelial tissue homeostasis and morphogenesis. *Science* **340,** 1185–1189 (2013).
2. Heisenberg, C. P. & Bellaiche, Y. Forces in tissue morphogenesis and patterning. *Cell* **153,** 948–962 (2013).
3. Leptin, M. & Grunewald, B. Cell shape changes during gastrulation in *Drosophila*. *Development* **110,** 73–84 (1990).
4. Sweeton, D., Parks, S., Costa, M. & Wieschaus, E. Gastrulation in *Drosophila*: the formation of the ventral furrow and posterior midgut invaginations. *Development* **112,** 775–789 (1991).
5. Dawes-Hoang, R. E. *et al.* Folded gastrulation, cell shape change and the control of myosin localization. *Development* **132,** 4165–4178 (2005).
6. Martin, A. C. & Goldstein, B. Apical constriction: themes and variations on a cellular mechanism driving morphogenesis. *Development* **141,** 1987–1998 (2014).
7. Walck-Shannon, E. & Hardin, J. Cell intercalation from top to bottom. *Nat. Rev. Mol. Cell Biol.* **15,** 34–48 (2014).
8. Bertet, C., Sulak, L. & Lecuit, T. Myosin-dependent junction remodelling controls planar cell intercalation and axis elongation. *Nature* **429,** 667–671 (2004).
9. Blankenship, J. T., Backovic, S. T., Sanny, J. S., Weitz, O. & Zallen, J. A. Multicellular rosette formation links planar cell polarity to tissue morphogenesis. *Dev. Cell* **11,** 459–470 (2006).
10. Irvine, K. D. & Wieschaus, E. Cell intercalation during *Drosophila* germband extension and its regulation by pair-rule segmentation genes. *Development* **120,** 827–841 (1994).
11. Sherrard, K., Robin, F., Lemaire, P. & Munro, E. Sequential activation of apical and basolateral contractility drives ascidian endoderm invagination. *Curr. Biol.* **20,** 1499–1510 (2010).
12. Rozbicki, E. *et al.* Myosin-II-mediated cell shape changes and cell intercalation contribute to primitive streak formation. *Nat. Cell Biol.* **17,** 397–408 (2015).
13. Nishimura, T., Honda, H. & Takeichi, M. Planar cell polarity links axes of spatial dynamics in neural-tube closure. *Cell* **149,** 1084–1097 (2012).
14. Hashimoto, H., Robin, F. B., Sherrard, K. M. & Munro, E. M. Sequential contraction and exchange of apical junctions drives zippering and neural tube closure in a simple chordate. *Dev. Cell* **32,** 241–255 (2015).
15. Munjal, A. & Lecuit, T. Actomyosin networks and tissue morphogenesis. *Development* **141,** 1789–1793 (2014).
16. Roh-Johnson, M. *et al.* Triggering a cell shape change by exploiting preexisting actomyosin contractions. *Science* **335,** 1232–1235 (2012).
17. Solon, J., Kaya-Copur, A., Colombelli, J. & Brunner, D. Pulsed forces timed by a ratchet-like mechanism drive directed tissue movement during dorsal closure. *Cell* **137,** 1331–1342 (2009).
18. He, L., Wang, X., Tang, H. L. & Montell, D. J. Tissue elongation requires oscillating contractions of a basal actomyosin network. *Nat. Cell Biol.* **12,** 1133–1142 (2010).
19. Mason, F. M. & Martin, A. C. Tuning cell shape change with contractile ratchets. *Curr. Opin. Genet. Dev.* **21,** 671–679 (2011).
20. Martin, A. C., Kaschube, M. & Wieschaus, E. F. Pulsed contractions of an actin-myosin network drive apical constriction. *Nature* **457,** 495–499 (2009).
21. Rauzi, M., Lenne, P. F. & Lecuit, T. Planar polarized actomyosin contractile flows control epithelial junction remodelling. *Nature* **468,** 1110–1114 (2010).
22. Munjal, A., Philippe, J. M., Munro, E. & Lecuit, T. A self-organized biomechanical network drives shape changes during tissue morphogenesis. *Nature* **524,** 351–355 (2015).
23. Simoes Sde, M. *et al.* Rho-kinase directs Bazooka/Par-3 planar polarity during *Drosophila* axis elongation. *Dev. Cell* **19,** 377–388 (2010).
24. Mason, F. M., Tworoger, M. & Martin, A. C. Apical domain polarization localizes actin-myosin activity to drive ratchet-like apical constriction. *Nat. Cell Biol.* **15,** 926–936 (2013).
25. Simoes Sde, M., Mainieri, A. & Zallen, J. A. Rho GTPase and Shroom direct planar polarized actomyosin contractility during convergent extension. *J. Cell Biol.* **204,** 575–589 (2014).
26. Kasza, K. E., Farrell, D. L. & Zallen, J. A. Spatiotemporal control of epithelial remodeling by regulated myosin phosphorylation. *Proc. Natl Acad. Sci. USA* **111,** 11732–11737 (2014).
27. Vasquez, C. G., Tworoger, M. & Martin, A. C. Dynamic myosin phosphorylation regulates contractile pulses and tissue integrity during epithelial morphogenesis. *J. Cell Biol.* **206,** 435–450 (2014).
28. Buchsbaum, R. J. Rho activation at a glance. *J. Cell Sci.* **120,** 1149–1152 (2007).
29. Li, X. *et al.* Gpr125 modulates Dishevelled distribution and planar cell polarity signaling. *Development* **140,** 3028–3039 (2013).
30. Ackerman, S. D., Garcia, C., Piao, X., Gutmann, D. H. & Monk, K. R. The adhesion GPCR Gpr56 regulates oligodendrocyte development via interactions with $G\alpha_{12/13}$ and RhoA. *Nat. Commun.* **6,** 6122 (2015).
31. Wu, S. Y., Shin, J., Sepich, D. S. & Solnica-Krezel, L. Chemokine GPCR signaling inhibits β-catenin during zebrafish axis formation. *PLoS Biol.* **10,** e1001403 (2012).
32. Zallen, J. A. & Wieschaus, E. Patterned gene expression directs bipolar planar polarity in *Drosophila*. *Dev. Cell* **6,** 343–355 (2004).
33. Pare, A. C. *et al.* A positional Toll receptor code directs convergent extension in *Drosophila*. *Nature* **515,** 523–527 (2014).
34. Costa, M., Wilson, E. T. & Wieschaus, E. A putative cell signal encoded by the folded gastrulation gene coordinates cell shape changes during *Drosophila* gastrulation. *Cell* **76,** 1075–1089 (1994).
35. Manning, A. J. & Rogers, S. L. The Fog signaling pathway: insights into signaling in morphogenesis. *Dev. Biol.* **394,** 6–14 (2014).
36. Manning, A. J., Peters, K. A., Peifer, M. & Rogers, S. L. Regulation of epithelial morphogenesis by the G protein-coupled receptor mist and its ligand fog. *Sci. Signal.* **6,** ra98 (2013).
37. Parks, S. & Wieschaus, E. The *Drosophila* gastrulation gene concertina encodes a G α-like protein. *Cell* **64,** 447–458 (1991).
38. Kolsch, V., Seher, T., Fernandez-Ballester, G. J., Serrano, L. & Leptin, M. Control of *Drosophila* gastrulation by apical localization of adherens junctions and RhoGEF2. *Science* **315,** 384–386 (2007).
39. Fox, D. T. & Peifer, M. Abelson kinase (Abl) and RhoGEF2 regulate actin organization during cell constriction in *Drosophila*. *Development* **134,** 567–578 (2007).
40. Nikolaidou, K. K. & Barrett, K. A Rho GTPase signaling pathway is used reiteratively in epithelial folding and potentially selects the outcome of Rho activation. *Curr. Biol.* **14,** 1822–1826 (2004).
41. Oldham, W. M. & Hamm, H. E. Heterotrimeric G protein activation by G-protein-coupled receptors. *Nat. Rev. Mol. Cell Biol.* **9,** 60–71 (2008).
42. Hanlon, C. D. & Andrew, D. J. Outside-in signaling—a brief review of GPCR signaling with a focus on the *Drosophila* GPCR family. *J. Cell Sci.* **128,** 3533–3542 (2015).
43. Huang, J., Zhou, W., Dong, W., Watson, A. M. & Hong, Y. From the Cover: directed, efficient, and versatile modifications of the *Drosophila* genome by genomic engineering. *Proc. Natl Acad. Sci. USA* **106,** 8284–8289 (2009).
44. Martin, A. C., Gelbart, M., Fernandez-Gonzalez, R., Kaschube, M. & Wieschaus, E. F. Integration of contractile forces during tissue invagination. *J. Cell Biol.* **188,** 735–749 (2010).
45. Fuse, N., Yu, F. & Hirose, S. Gprk2 adjusts Fog signaling to organize cell movements in *Drosophila* gastrulation. *Development* **140,** 4246–4255 (2013).
46. Mathew, S. J., Kerridge, S. & Leptin, M. A small genomic region containing several loci required for gastrulation in *Drosophila*. *PLoS ONE* **4,** e7437 (2009).
47. Gong, W. J. & Golic, K. G. Ends-out, or replacement, gene targeting in *Drosophila*. *Proc. Natl Acad. Sci. USA* **100,** 2556–2561 (2003).
48. Morize, P., Christiansen, A. E., Costa, M., Parks, S. & Wieschaus, E. Hyperactivation of the folded gastrulation pathway induces specific cell shape changes. *Development* **125,** 589–597 (1998).
49. Chen, Z. *et al.* Activation of p115-RhoGEF requires direct association of Gα13 and the Dbl homology domain. *J. Biol. Chem.* **287,** 25490–25500 (2012).

METHODS

Differential interference contrast live imaging. Standard techniques were used to immobilize embryos for imaging. Phase-contrast time-lapse images were collected on an inverted microscope (Zeiss) and a programmable motorized stage to record different positions over time (Mark&Find module from Zeiss). The system was run with AxioVision software (Zeiss) and allowed the acquisition of time-lapse data sets in wild-type, mutant or injected embryos. From these DIC videos the extent of elongation was measured 40 min post dorsal movement of the posterior pole cells.

Fixation of embryos, *in situ* hybridization. Embryos were fixed with 4% formaldehyde in PBS and stored in methanol before staining with fluorescent dysoxygenin antisense mRNA probes to *smog* using established protocols.

RNA interference. dsRNA probes against *CG31660* (*smog*) were made using PCR products containing the sequence of the T7 promoter (5′-TAATACGACTCACTA TAGG-3′) followed by 18–21 nucleotides specific to the gene. Probe 1, located in the 5′-UTR, targets nucleotides 2–602 of *CG31660*-RC (GenBank ID: NM_001014465). Probe 2, coding probe, located adjacent to the ATG, targets nucleotides 636–1,181. Gel-purified PCR products were subsequently used as a template for the *in vitro* RNA synthesis with T7 polymerase using Ribomax (Promega, P1300). The dsRNA probes were purified using Sure-Clean (Bioline, BIO-37047), precipitated, washed and resuspended in RNase-free water, quantified by OD, checked on agarose gel and diluted for injection at 5 µM concentration.

RNAi *fog* probes were described previously[7].

Ends-out gene targeting at the *CG31660* locus. To carry out homologous recombination, producing an 11,053 bp deletion in the *CG31660* locus called *smog*, we used the Ends-Out technique[46]. Left (LA) and right (RA) homology arms, respectively of 3,243 bp and 3,272 bp, were PCR amplified using the following respective primer pairs and genomic DNA from *y w* flies as matrix. 5′-AGC AGCGGCCGCGTCTGCACTGGGTAACGTGAATTTG+TACCGGTACCCGAT TGAGCGGACCGTTTCGATTAC-3′ and 5′-AGCAGGCGCGCCCACACAATGT ACGAGGACGAAAGCG+TACCCGTACGGTTCCACTGCGGTTACTGCGAG AAG-3′. LA is located 5′ to the start codon (3,684 to 441 bp before); RA, 830 bp 3′ to the stop codon (830 to 4,102 bp after) of pog-RB (FlyBase *CG31660*). LA was cloned using NotI+Acc65I and RA AscI+BsiWI into the pW25 vector[46]. *y w* flies were transformed using standard procedures. Insertions were genetically localized and a third chromosome donor DNA was crossed to *hs-flp hs-ISceI /CyO* and heat shocked to excise and to linearize the *CG31660*-targeting molecule as described previously[46]. Putative deletion events were selected by homozygous sterility and localization to chromosome 2.

Three complementary experiments were undertaken to verify the *smog* deletion. First, genomic PCR amplification of the modified locus: gDNA purified from homozygous KO flies using the blood & cell culture DNA mini kit (Qiagen, 13323) was PCR amplified with primers located outside the recombined locus (5′-CG CAGCCATTCTCCACTTTTGT-3′ and 5′-atcgtggctgttttgcaggaga-3′) using the Expand long-template Taq polymerase (Roche, 4743814001). The corresponding genomic PCR fragment of 11.3 kbp, entirely sequenced, confirms integration of the donor DNA cassette at the locus (sequence available on request). Second, RT–qPCR was performed to verify the absence of any mRNAs transcribed from the *smog* locus (Supplementary Fig. 3a). Total RNA extraction from early gastrulating embryos homozygous for *smog* or *y w* was performed using the RNeasy mini kit (QIAGEN, 74104) with an additional DNAseI treatment step to remove genomic DNA contamination. Retrotranscription was performed with the iScript Reverse Transcription Supermix (Bio-RAD, 170-8841) according to the manufacturer's protocol. Real-time PCR was performed on a CFX96 qPCR detection system (Bio-RAD) with the following TaqMan probes (TaqMan Gene Expression Assays from Life Technologies) plus TaqMan Gene expression master mix, following the classical TaqMan protocol: *E3*: Dm01846328_m1= probe located in E3 (exon 3-4 boundary, 1431/GenBank NM_001014465, amplicon = 69 bp); *RPII140:* House-keeping gene reference: Dm02134593_g1 (exon 2-3 boundary, 2331/GenBank BT003265, amplicon = 78 bp);

RT–qPCR conditions were as follows: 40 cycles of 95 °C for 15 s and 60 °C for 60 s.

Analyses were performed in triplicate from three independent experiments. Transcript levels were first normalized to the house-keeping gene *RPII140*; and then to the *y w* control group. The ΔΔCq method was used to estimate relative amounts using the Bio-RAD CFX manager software. A 125-fold depletion of *smog* transcripts was observed in homozygous KO embryos compared with *y w* control embryos.

Third, genomic-qPCR was performed to verify the absence of any wild-type *smog* DNA (Supplementary Fig. 3b). Real-time PCR was performed on a CFX96 qPCR detection system (Bio-RAD) with the following homemade TaqMan probes located in either the disrupted E3 or E14 exon of *smog* and 3′ to the deletion as control: *E3: F*: 5′-AGCAGCACTAAAAGCAGTAA-3′; R = 5′-CCGACTATCAAAAGCA CCAG-3′, FamTam probe: 5′-CAGCAGCACACAATTAAACACCC-3′, amplicon: 98 bp; *E14: F*: 5′-GGACCCACGGATACCTATG-3′; R: 5′-ATACAATTCTCA AATATCCGCC-3′, FamTam probe: 5′-ACCAGCAAGGACTCCCTACTTC-3′, amplicon: 137 bp; control: F: 5′-ATATTGCTTGGCTACCCTC-3′; R: 5′-TAATC AAGCGTCTAGTTCGAGT-3′, FamTam probe: 5′-ATTTCCAGCAAGTGACATT CGG-3′; amplicon: 199 bp.

Q-gPCR conditions were as follows: 40 cycles of 95 °C for 15 s and 55 °C for 60 s.

Analyses were performed in duplicate. Genomic DNA level was first normalized using the TaqMan amplicon control located in the non-deleted 3′ part of the locus and then to the *y w* flies. The ΔΔCq method was used to estimate relative amounts using the Bio-RAD CFX manager software. A 48-fold depletion for *E3* TaqMan probes and a 71-fold depletion for *E14* TaqMan probes were observed in *smog* homozygotes compared with *y w* control flies.

The pog^{1} mutation[45] was incorrectly ascribed to *CG31660* (FlyBase) because it complements the *smog* deletion produced here.

Fly constructs and genetics. The following mutant chromosomes were used: cta^{RC10}, fog^{4a6} (ref. 47), *FRTG13 Gγ1* (refs 49,50) *pUAST–fog6*, *UAS–fog12* (ref. 5), *pUAST–ctaQ303L* (ref. 44), *UAS–TRIP Mist* (Bloomington 41930), *UAS–TRIP RhoGEF4* (Bloomington 42550) and *UAS–TRIP RhoGEF2* (Bloomington 34643; ref. 51). *endoCAD::GFP* replaces endogenous E-cadherin protein at the locus[42] and *sqh–RLCMyosinII::mCherry* (chromosome 2 or 3; ref. 19). *sqh–Rok K116A::GFP* (ref. 22). *nos–Gal4* and *67–Gal4* (*matα4-GAL–VP16*) are ubiquitous, maternally supplied, Gal4 drivers. *ubi–Rok::GFP* (ref. 52).

Germline clones for *Gγ1*, $Gβ13F^{Δ1\text{-}96A}$ (ref. 53), $RhoGEF2^{l(2)04291}$ (ref. 54) and *smog* were made using the FLP-DFS system[55]).

All fly constructs and genetics are listed in Supplementary Extended Table 1.

Constructs and transgenes. RE70685 (GenBank, BT003470), which corresponds to the B form of Smog (pog-RB in FlyBase, Supplementary Fig. 1), was used as a matrix to build the first constructs after correction of a TT deletion located after P405 that resulted in a frameshift, using the Quick-change site-directed Mutagenesis kit (Agilent, 200555). The ORF (2,370 bp) without the stop codon was then PCR amplified and cloned into the GATEWAY entry clone pDONR (Life Technologies) following the manufacturer's BP cloning protocol, resulting into p221–Smog-B. This plasmid was modified using classical methods to obtain also the longer ORF of the C form (pog-RC in FlyBase), p221-Smog-C. Both p221 plasmids were recombined with a pCasper4–*sqh* promoter Cter EGFP-tagged destination vector using GATEWAY LR cloning to obtain the expression vector *sqh–smog*C::*GFP*.

Rho1 sensor *Ubi–GFP::AniRBD* and *sqh–sqhEE::GFP* are described in ref. 21. All recombinant expression vectors were verified by sequence (Beckman) and were sent to BestGene for PhiC31 site-specific-mediated insertion or random site transgenesis. FASTA sequences of these vectors are available on request.

Image acquisition. Embryos were prepared as described before[56]. Time-lapse imaging was initiated before cephalic furrow formation (presumptive mesoderm for 10–15 min) or from stage 7 to stage 8 (ventral–lateral ectoderm; 15–30 min depending on the experiment) on a PerkinElmer inverted microscope using a ×100 objective for Figs 1, 3–6 and Supplementary Extended Fig. 1. RLCMyosinII::mCherry and endoCad::GFP were captured every 6–7 s on 7–10 *Z* planes, separated by 0.5 µm, using 200 mS capture and 50% power on the green and 300 mS capture with 60% power on the red channel. A Nikon spinning-disc Eclipse Ti inverted microscope using a ×100, 1.4 N.A oil immersion objective at room temperature (~22 °C) was used for Fig. 6 and Supplementary Figs 4 and 5. The system acquires images using the MetaMorph software. Seven *z*-sections, 0.5 µm apart, were acquired every 5 s using a single camera. Laser power was measured and kept constant between experiments.

Image analysis. All image processing was done in Fiji freeware software. For all quantifications, maximum-intensity *z*-projection of slices was used, followed by a background subtraction using the available plugin in Fiji. For junctional intensity and planar polarity measurements, regions were drawn manually. For pulsatility measurements, individual cells were tracked using CellTrack1.1 (open source software). The procured region was shrunken using a constant thickness to exclude contribution from junctional signals. Medial intensity time traces were smoothened to automatically calculate pulse amplitude and frequency using the Igor Pro (Wavemetrics).

S2 cell experiments (baculoviral production of Fog and antibody staining). *pVLHis ::fog ::AP* and *pVLfog ::AP* (gift from K. Zinn, Caltech, USA) were recombined with the viral Bacmid in DH10Bac bacteria. SF9 cells were then transfected with viral DNA to produce the tagged ligand. Medium was collected, assayed for Fog on westerns with rabbit anti-Fog (gift from N. Fuse) and stored at 4 °C. *Drosophila* Schneider S2 cells, cultured in Insect-Xpress medium (Whittaker), were transfected with *Actin–Gal4* and *pTWUAS- pTWUAS-SmogC::GFP* plasmids.

DOI: 10.1038/ncb3302

Cells were transiently transfected with 500 ng of DNA per construct using 10 µl Cellfectin reagent (Invitrogen). After 24 h the transfection mix was removed, medium and cover slides coated with 0.5 mg ml^{-1} concanavalin were added and the expression of transfected constructs induced with 1 mM $CuSO_4$. Cells were incubated for another 24 h. The medium was then replaced with Fog::AP medium or medium for 2 h, removed and rinsed in PBS 0.1% Tween20, then fixed with 8% formaldehyde in PBS for 10 min. After washing with PBS 0.1% Tween20, a standard antibody staining was performed.

Antibodies were: rabbit anti-Fog (ref. 44; 1:1,000), chicken anti-GFP (AVES GFP-120 1:500), Alexa555 anti-rabbit (MoBiTec; 1:500). Cells were mounted on slides in Aquamount and analysed with a Zeiss LSM confocal microscope.

Dextran and drug injection. Dextran 568 (1 mg ml^{-1}; 10,000 daltons; Life Technology) was injected into the perivitelline space of *67-Gal4/+*; *sqh–SmogC::GFP/+* and *67-Gal4/ UAS–fog12*; *sqh–SmogC::GFP/+* embryos at the end of cellularization. H1152 (Enzo Life Sciences) was injected in Stage 5a embryos at 10 mM for strong inhibition, and at 5 mM for weaker inhibition in Fig. 8. Water injections were used as controls.

Statistics. Average values are calculated from n, where n is the number of embryos/cells/pulses as noted in the figure. This number was used for conducting statistical significance tests. In planar polarity and junctional intensity measurements, n is the number of embryos. Error bars usually depict s.e.m. (that is, s.d./$\sqrt{n}$, where n is the number of embryos, unless otherwise mentioned) or s.d. Non-parametric Mann–Whitney U-test was performed in Origin (v8) to calculate the P values. No statistical method was used to predetermine sample size. The experiments were not randomized, and the investigators were not blinded to allocation during experiments and outcome assessment.

Repeatability. All measurements were performed in 2–15 embryos and repeated at least twice.

50. Izumi, Y., Ohta, N., Itoh-Furuya, A., Fuse, N. & Matsuzaki, F. Differential functions of G protein and Baz-aPKC signaling pathways in *Drosophila* neuroblast asymmetric division. *J. Cell Biol.* **164,** 729–738 (2004).
51. Kanesaki, T., Hirose, S., Grosshans, J. & Fuse, N. Heterotrimeric G protein signaling governs the cortical stability during apical constriction in *Drosophila* gastrulation. *Mech. Dev.* **130,** 132–142 (2013).
52. Ni, J. Q. *et al.* A genome-scale shRNA resource for transgenic RNAi in *Drosophila*. *Nat. Methods* **8,** 405–407 (2011).
53. Bardet, P. L. *et al.* PTEN controls junction lengthening and stability during cell rearrangement in epithelial tissue. *Dev. Cell* **25,** 534–546 (2013).
54. Schaefer, M., Petronczki, M., Dorner, D., Forte, M. & Knoblich, J. A. Heterotrimeric G proteins direct two modes of asymmetric cell division in the *Drosophila* nervous system. *Cell* **107,** 183–194 (2001).
55. Hacker, U. & Perrimon, N. DRhoGEF2 encodes a member of the Dbl family of oncogenes and controls cell shape changes during gastrulation in *Drosophila*. *Genes Dev.* **12,** 274–284 (1998).
56. Chou, T. B. & Perrimon, N. Use of a yeast site-specific recombinase to produce female germline chimeras in *Drosophila*. *Genetics* **131,** 643–653 (1992).

nature cell biology

DOI: 10.1038/ncb3302

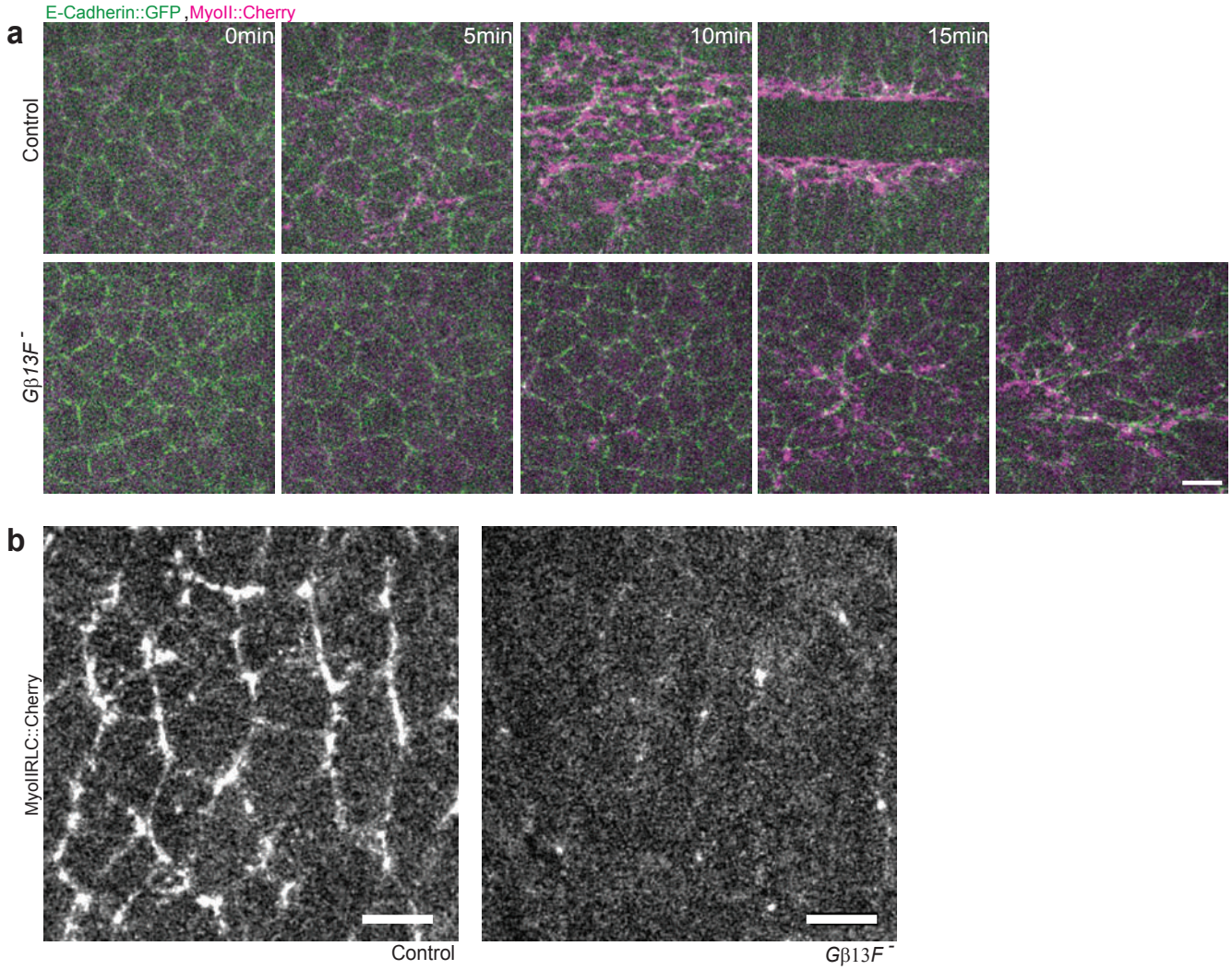

Supplementary Figure 1 Gb13F is required for apical MyoII accumulation. MyoII in control and *Gb13F* mutant mesoderm (a) and ectoderm (b). Scale bars 10μm (a) and 5μm (b).

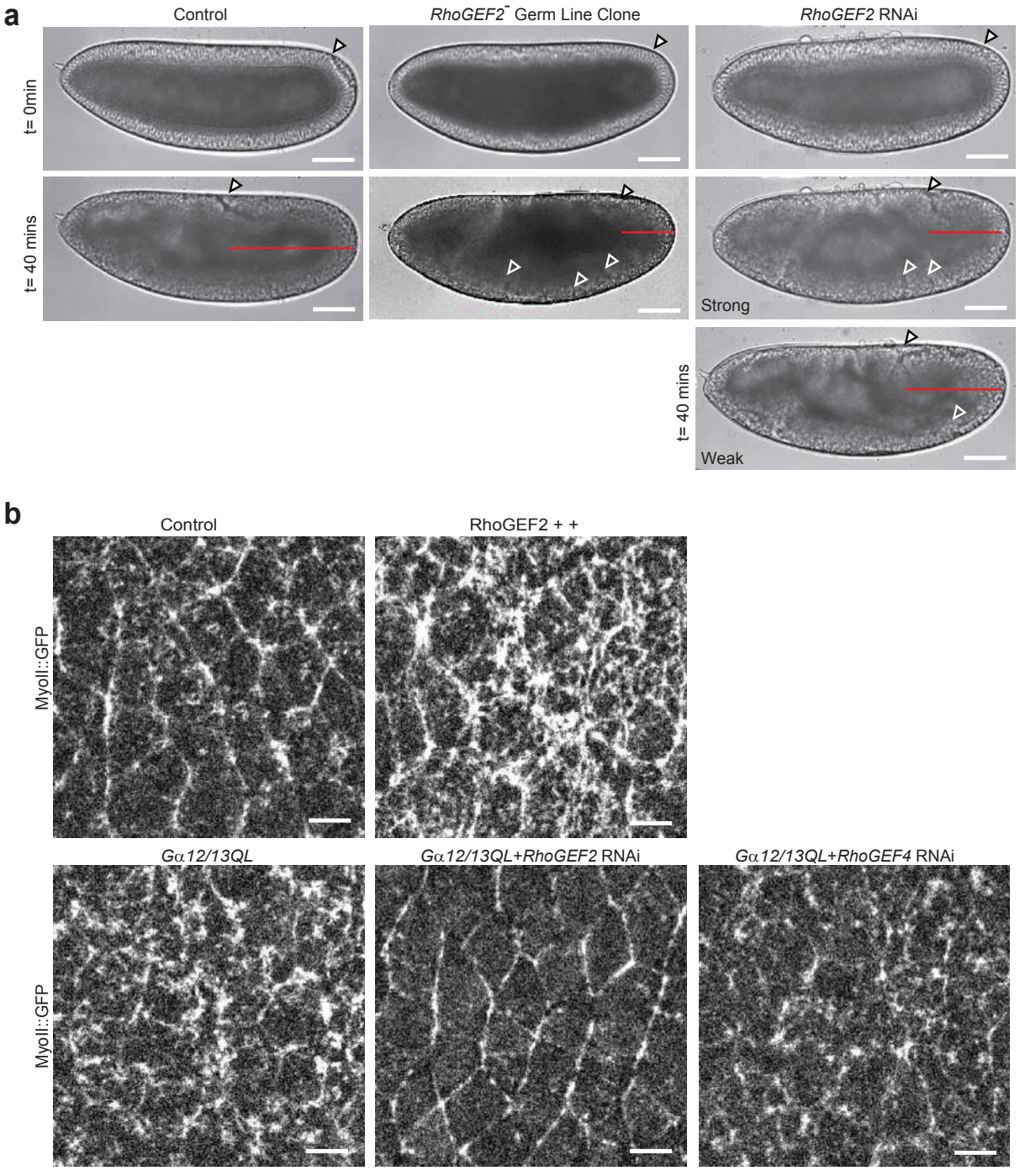

Supplementary Figure 2 RhoGEF affects elongation. Embryos showing elongation defects in mutant *RhoGEF2* and RNAi compared to controls (a). Arrow heads point to the dorsal edge of posterior midgut at indicated times and red lines highlight the extent of elongation at indicated time. Note the folds in ectoderm (white arrows) b) MyoII::GFP levels in controls and RhoGEF2 over-expression (c) MyoII::GFP levels in $G\alpha_{12/13}$*QL303 plus RhoGEF4 RNAi* (right panel compared to $G\alpha_{12/13}$*QL303 (left)* and $G\alpha_{12/13}$*QL303* plus *rhoGEF2 RNAi* (middle). Scale bars 100μm (a)and 5μm (b).

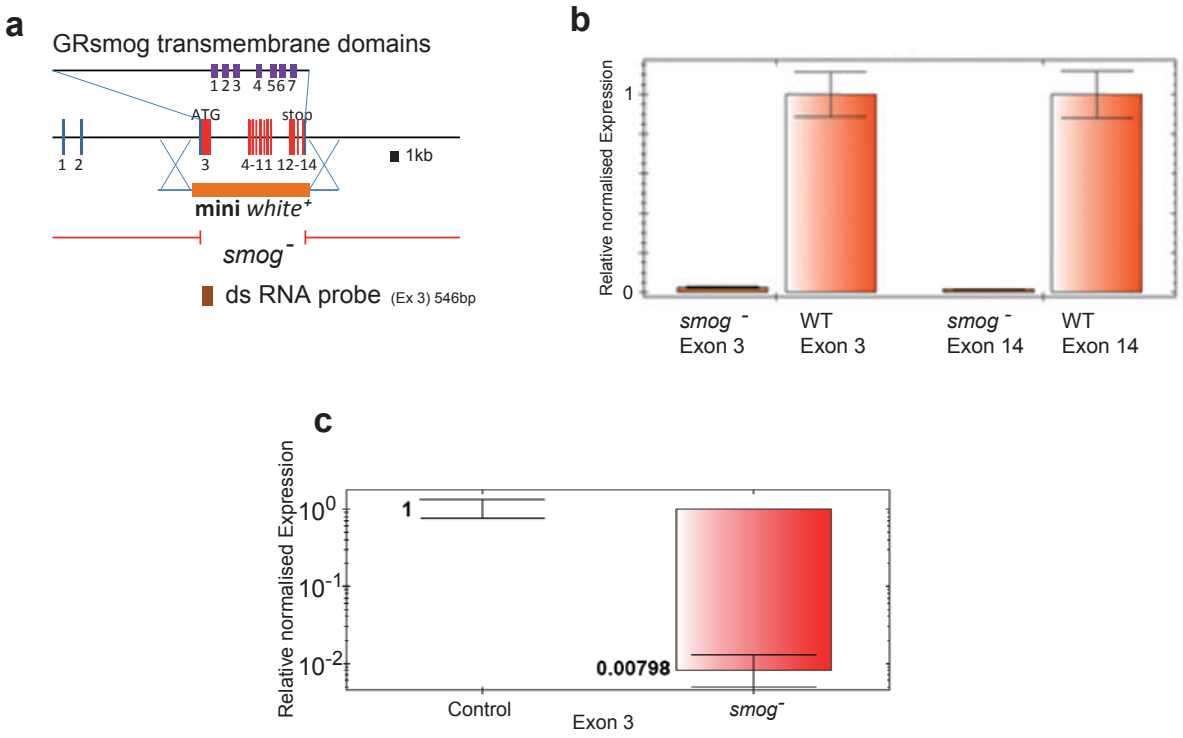

Supplementary Figure 3 *Smog* gene structure, knock out and RNAi probe. **a)** *CG31660* gene structure encoding for Smog. Red boxes: coding exons, blue boxes: 5' and 3' non coding exons. The predicted 7 pass transmembrane regions are depicted above. Smog disrupting dsRNA probe below in brown. The deleted portion of the knockout of *smog* between red lines. b) Real time QPCR using gDNA showing that *smog* knock out lacks the WT locus (see Materials and Methods) ; n=3 independent experiments. c) RT-QPCR showing the specific absence of mRNAs transcribed from the *smog* knock out. (see Materials and Methods); n=3 independent experiments. Error bars are Standard Error of Mean.

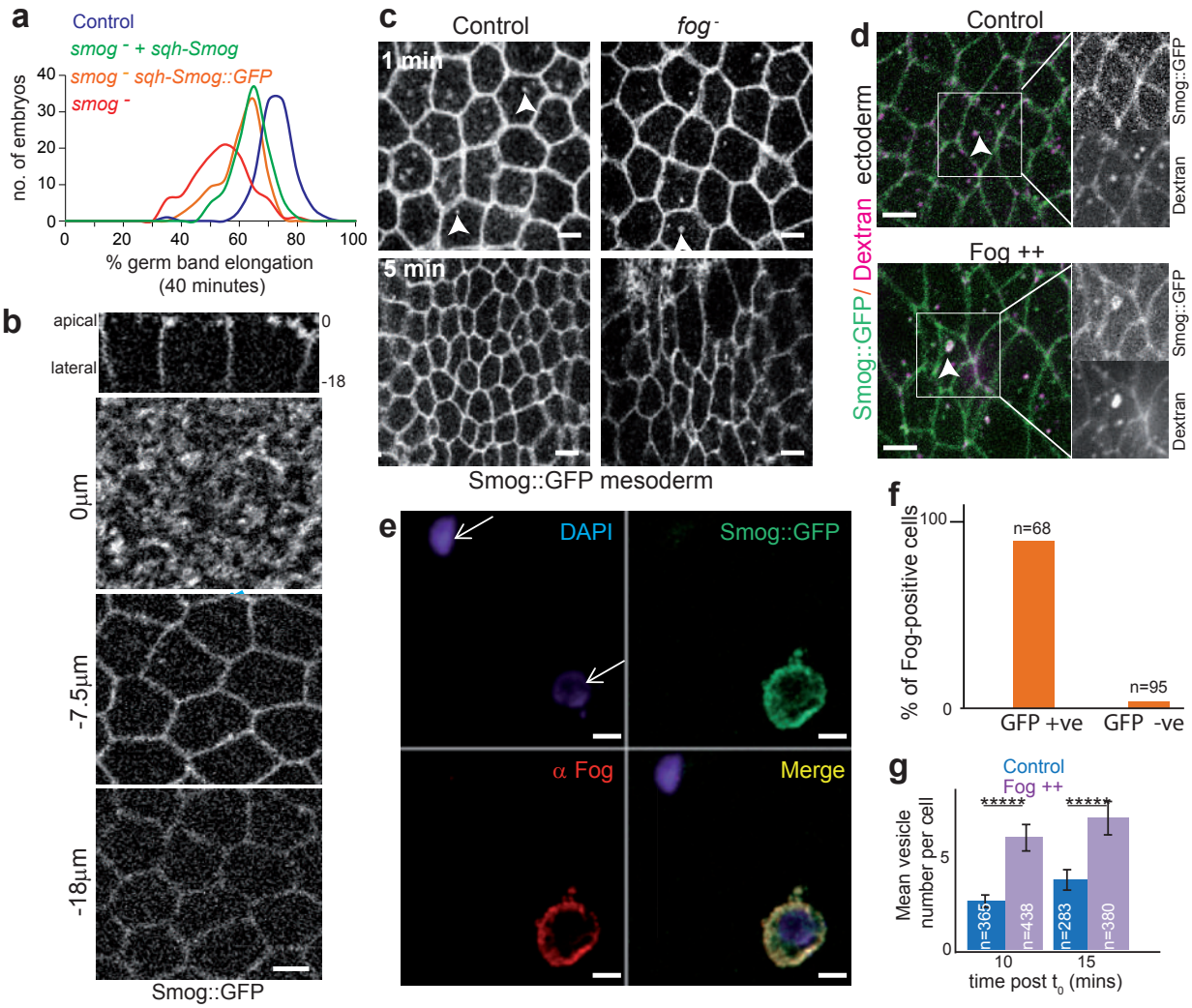

Supplementary Figure 4 Fog induces endocytosis of Smog and is immobilized on heterologous cells expressing Smog::GFP. a) partial rescue of the *smog*⁻ elongation phenotype by sqh-driven production of Smog and Smog::GFP. b) Functional Smog::GFP is detected at the surface of epithelial cells: top orthogonal view lower panels single planes c) Smog::GFP is also detected in intracellular organelles in mesoderm cells (left top, arrowheads). Loss of zygotic Fog reduces Smog::GFP positive organelles in mesoderm cells (top right) prior to constriction (**d**) Smog::GFP (green) is detected together with extracellular -injected dextran (magenta) at the surface and in intracellular organelles in the ectoderm during intercalation (top panel). Overexpression of Fog increases intracellular Smog::GFP positive organelles (bottom panel, quantified in (g) where n = number of embryos and ***** is p<0.000005). Vesicle sizes are often larger in cells over-expressing Fog (d enlarged in right panels). (e) Fog (red) is immobilised on the surface of S2 cells expressing Smog::GFP (green); quantified in (f) n=68 (GFP positive) and 95 (GFP negative) cells. Error bars are Standard Error of Mean. Scale bars 5µm

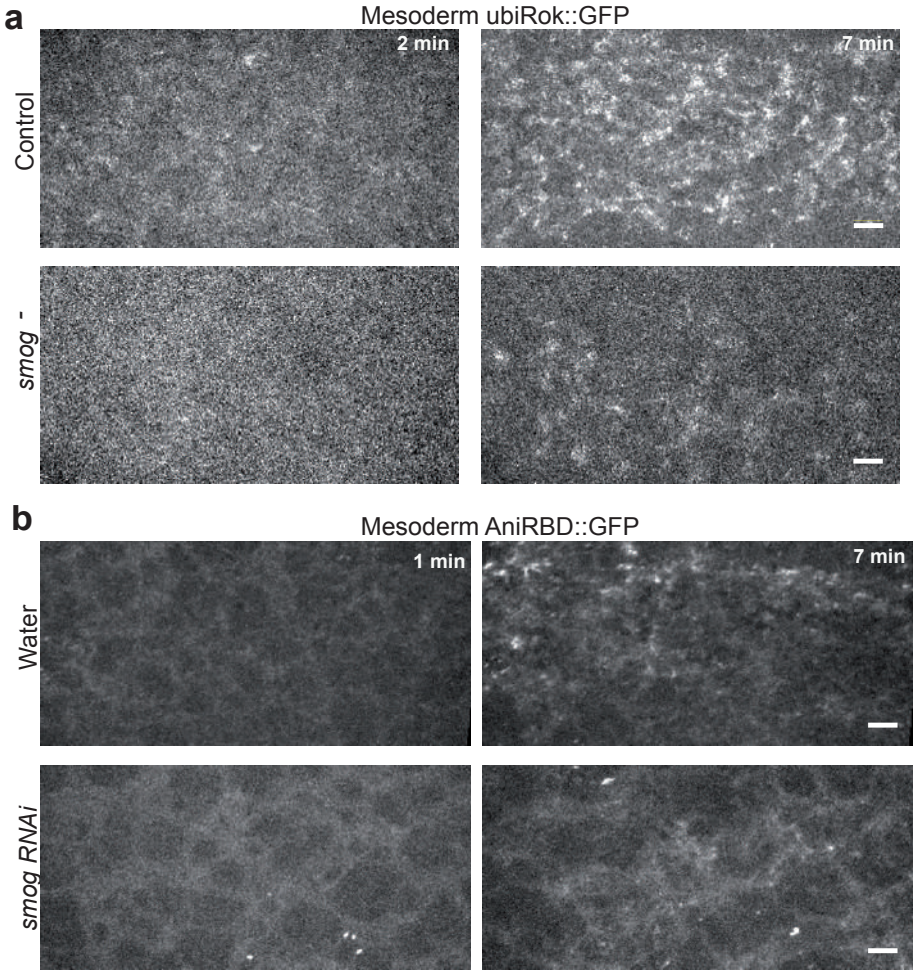

Supplementary Figure 5 Smog is required for apical accumulation of Rok and Rho1 in the mesoderm. Ubi-Rok::GFP (a) and Rho biosensor::GFP distribution in mesoderm cells at indicated times in control and *smog* mutants. Scale bars 5μm.

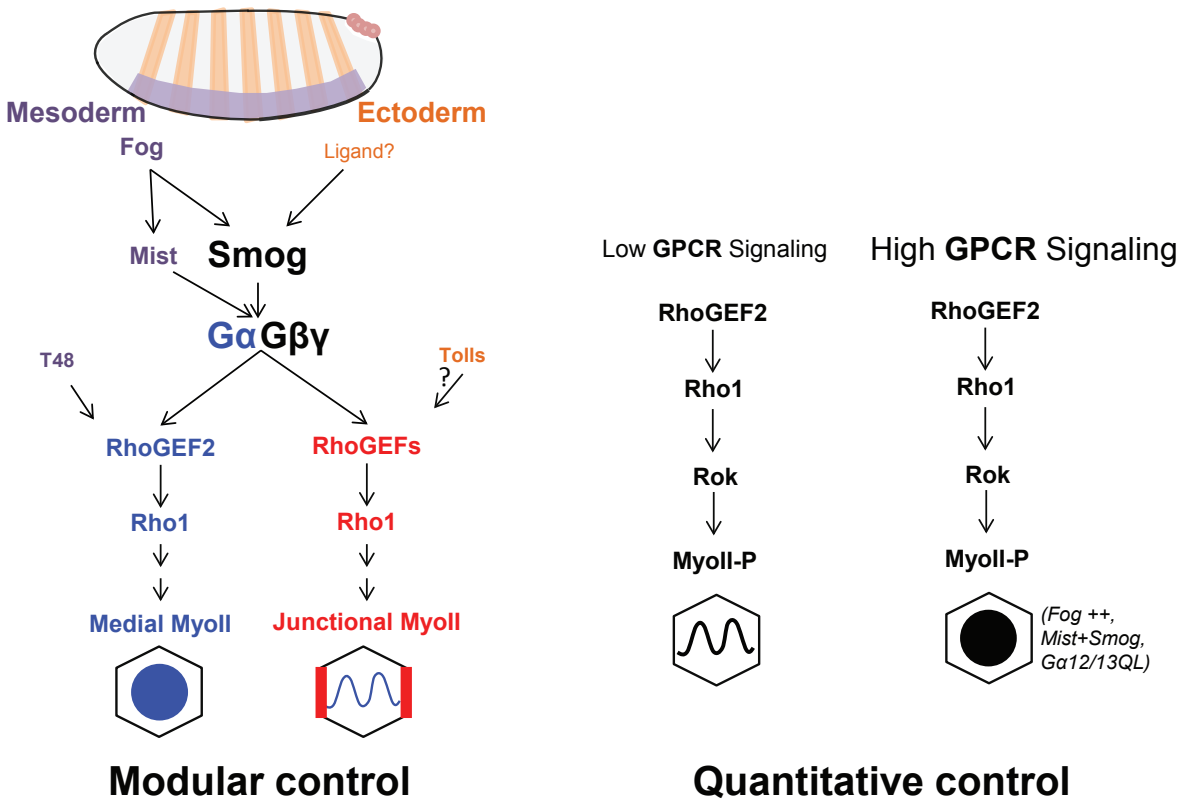

Supplementary Figure 6 Models for modular and quantitative control of MyoII activation. Localised inputs derive from striped ectoderm (orange) and ventral mesoderm (purple) expressed transcription factors in blastoderm embryos (top). Mesoderm and endoderm patterning relies on Fog and possibly other ligands signalling via multiple, localised (e.g. Mist) or ubiquitous (e.g. Smog) GPCRs, which relay information to G proteins α, β and γ. T48 and Tolls are single pass transmembrane proteins.

Figure	Cross or genotype
1a, i, 5a, e movies 1,4	*sqh^{AX3} /+; sqh-RLCMyosinII::mCherry endoCAD::GFP / sqh-RLCMyosinII::mCherry endoCAD::GFP*
1b , j movies 1, 4	*y w hsflp / +; FRTG13 Gγ1^{f159} sqh-RLCMyosinII::mCherry endoCad::GFP/ FRTG13 ovo^{D} x FRTG13 Gγ1^{e159} sqh-RLCMyosinII::mCherry endoCad::GFP/CyO (Germ line clones)*
1c k movies 2, 5	*sqh^{AX3} /+; cta^{BC10} sqh-RLCMyosinII::mCherry endoCAD::GFP / cta^{BC10} sqh-RLCMyosinII::mCherry endoCAD::GFP*
Supplementary 1 a, b movies 3, 6	*Gβ13F^{e1-96A} FRT9-2/ovo^{D2} FRT9-2; sqh-RLCMyosinII::mCherry endoCad::GFP/hs-flp38 x y w* (germ line clones; paternal rescue control) Or *Y* (experiment)
2a	*67-Gal4 sqh-RLCMyosinII::GFP/+ x y w*
2b	*67-Gal4 sqh-RLCMyosinII::GFP/+; UAS-TRIPRhoGEF2* (BL 34643) *x y w*
2c Supplementary 2b (bottom left)	*67-Gal4 sqh-RLCMyosinII::GFP/+; x UAS-ctaQL/TM3*
2d Supplementary 2b (bottom middle)	*67-Gal4 sqh-RLCMyosinII::GFP/+; UAS-TRIPRhoGEF2* (BL 34643)/+ *x UAS-ctaQL/TM3*
Supplementary 2a (middle)	*hs-flp /+; FRTG13 RhoGEF2^{EG04230}/FRTG13 ovo^{D}; x RhoGEF2^{102062}/CyO* (germ line clones)
Supplementary 2a (right)	*67-Gal4 /+; UAS-TRIPRhoGEF2* (BL 34643) *x y w*
Supplementary 2b (bottom right)	*67-Gal4 sqh-RLCMyosinII::GFP/+; UAS-TRIPRhoGEF4* (BL 42550)/+ *x UAS-ctaQL/TM3*
Supplementary 2b (top right)	*67-Gal4 sqh-RLCMyosinII::GFP /+; UAS-RFP::RhoGEF2/+ x +/+*
3a	*endo-Cad::GFP* (top), *smog endo-Cad::GFP/ smog endo-Cad::GFP* (middle), *cta^{BC10} endo-Cad::GFP/ cta^{BC10} endo-Cad::GFP* (bottom)
	y w (top), *smog/smog* (2nd row), *cta^{BC10} /cta^{BC10}* (3rd row), *Gγ1^{e159}* germ line clones (4th row), *Gβ13F^{01-}*
3c	*^{96A}* germ line clones (5th row)
4a, c, d, f, 6f-i, movies 7 and 8	*67-Gal4 sqh-RLCMyosinII::mCherry endoCAD::GFP* /67-Gal4 *sqh-RLCMyosinII::mCherry endoCAD::GFP x y w*
4b, e, g, movies 7 and 8	*67-Gal4 sqh-RLCMyosinII::mCherry endoCAD::GFP* /67-Gal4 *sqh-RLCMyosinII::mCherry endoCAD::GFP x UAS-TRIPMist/ UAS-TRIPMist* (BL 41930)
Supplementary 4b	*smog/smog; sqh-smog::GFP/sqh-smog::GFP*
Supplementary 4c (right)	*fog^{4x}/Y ; sqh-smog::GFP/sqh-smog::GFP*
Supplementary 4c (left)	*sqh-smog::GFP/sqh-smog::GFP*
Supplementary 4d	*67-Gal4/+; sqh-smogC::GFP/ sqh- smogC::GFP* x *UAS-fog6/+*
5b, f, movie 9	*y w cv sqh^{AX3}/+; smog sqh-RLCMyosinII::mCherry endoCAD::GFP / smog sqh-RLCMyosinII::mCherry endoCAD::GFP.*
Supplementary 5a (top)	*ubi-Rok::GFP /+ x +/+*
Supplementary 5a (bottom)	*smog/smog; ubiRok::GFP/+ x smog/smog*
Supplementary 5b	*ubiRok::GFP sqh-RLCMyosinII::mCherry/ ubiRok::GFP sqh-RLCMyosinII::mCherry*
5j	*sqh-RLCMyosinII::mCherry endoCAD::GFP / sqh-RLCMyosinII::mCherry endoCAD::GFP; nos-Gal4/nos-Gal4 x sqh-RLCMyosinII::mCherry endoCAD::GFP / sqh-RLCMyosinII::mCherry endoCAD::GFP*
5k	*sqh-RLCMyosinII::mCherry endoCAD::GFP / sqh-RLCMyosinII::mCherry endoCAD::GFP; nos-Gal4/nos-Gal4 x sqh-RLCMyosinII::mCherry endoCAD::GFP / sqh-RLCMyosinII::mCherry endoCAD::GFP; UAS-fog6/+*
5l	*smog sqh-RLCMyosinII::mCherry endoCAD::GFP / smog sqh-RLCMyosinII::mCherry endoCAD::GFP; nos-Gal4/nos-Gal4 x smog sqh-RLCMyosinII::mCherry endoCAD::GFP / smog sqh-RLCMyosinII::mCherry endoCAD::GFP; UAS-fog6/+*
5m	*cta^{BC10} sqh-RLCMyosinII::mCherry endoCAD::GFP / cta^{BC10} sqh-RLCMyosinII::mCherry endoCAD::GFP; nos-Gal4/nos-Gal4 x cta^{BC10} sqh-RLCMyosinII::mCherry endoCAD::GFP / cta^{BC10} sqh- RLCMyosinII::mCherry endoCAD::GFP; UAS-fog6/+.*
6a	*sqh-RokK116A::GFP/ sqh-RokK116A::GFP; sqh-RLCMyosinII::mCherry / sqh-RLCMyosinII::mCherry*
6b	*ubi-anilinRBD::GFP sqh-RLCMyosinII::mCherry /ubi-anilinRBD::GFP sqh-RLCMyosinII::mCherry*
6g	*sqh-RLCMyosinII T20ES21E::GFP/sqh- RLCMyosinII T20ES21E::GFP*
6j, movie 10	*sqh-RLCMyosinII::mCherry endoCAD::GFP/ sqh-RLCMyosinII::mCherry endoCAD::GFP*

Supplementary Table 1 Summary of genotypes employed.

Legends to Supplementary Videos

Video 1 Developing mesoderm in control and *Gγ1* mutant. MyoII::Cherry (magenta) and E-cadherin::GFP (green); Scale =5μm.

Video 2 Developing mesoderm in control and *Gα*12/13 mutant. MyoII::Cherry (magenta) and E-cadherin::GFP (green); Scale =5μm.

Video 3 Developing mesoderm in control and *Gαβ13F* mutant. MyoII::Cherry (magenta) and E-cadherin::GFP (green); Scale =5μm.

Video 4 Developing ectoderm in control and *Gγ1* mutant. MyoII::Cherry (magenta) and E-cadherin::GFP (green) on left and MyoII::Cherry on right ; Scale =5μm.

Video 5 Developing ectoderm in control and *Gα*12/13 mutant. MyoII::Cherry (magenta) and E-cadherin::GFP (green) on left and MyoII::Cherry on right; Scale =5μm.

Video 6 Developing ectoderm in control and *Gβ13F* mutant. MyoII::Cherry (magenta) and E-cadherin::GFP (green) on left and MyoII::Cherry on right; Scale =5μm.

Video 7 Developing mesoderm in control, *smog* RNAi, *mist* RNAi and *smog+mist* double RNAi embryos. MyoII::Cherry (magenta) and E-cadherin::GFP (green); Scale =5μm.

Video 8 Developing mesoderm in control, *fog* RNAi, *mist+fog* RNAi and *smog+fog* double RNAi embryos. MyoII::Cherry (magenta) and E-cadherin::GFP (green); Scale =5μm.

Video 9 Developing ectoderm in control and *smog*$^{-}$ mutant. MyoII::Cherry (magenta) and E-cadherin::GFP (green) on left and MyoII::Cherry on right; Scale =5μm.

Video 10 Developing mesoderm in control, H1152 5mM and H1152 10mM injected embryos. MyoII::Cherry (green) and E-cadherin::GFP (purple); Scale =5μm.